Genome-wide effects of the antimicrobial peptide apidaecin on translation termination

Kyle Mangano[1,2,#], Tanja Florin[1,#], Xinhao Shao[2], Dorota Klepacki[1], Irina Chelysheva[3], Zoya Ignatova[3], Yu Gao[2], Alexander Mankin[1,2*] and Nora Vázquez-Laslop [1,2*]

[1] Center for Biomolecular Sciences, University of Illinois at Chicago, Chicago, IL 60607, USA

[2] Department of Pharmaceutical Sciences, University of Illinois at Chicago, Chicago, IL 60612, USA

[3] Institute of Biochemistry and Molecular Biology, University of Hamburg, 20146 Hamburg, Germany

# these authors contributed equally to this work

* corresponding authors

Editorial correspondence:

Prof. Nora Vázquez-Laslop [1,2*]

Center for Biomolecular Sciences – m/c 870
University of Illinois at Chicago
Chicago, IL 60607, USA
email:nvazquez@uic.edu
phone: 312-996-4005
FAX: 312-413-9303

keywords: antibiotic, antimicrobial peptide, translation, termination, stop codon bypass, protein synthesis, release factor

Abstract

Biochemical studies had shown that the antimicrobial peptide apidaecin (Api) inhibits protein synthesis by binding in the nascent peptide exit tunnel and trapping the release factor associated with a terminating ribosome. The mode of Api action in bacterial cells had remained unknown. Genome-wide analysis revealed that Api leads to pronounced ribosome arrest at stop codons and ribosome queuing. In addition, Api causes a dramatic increase of stop codon bypass by ribosomes paused in a pre-release state, resulting in accumulation of proteins with C-terminal extensions. Stop codon bypass occurs in 0-frame, by misincorporating near-cognate aminoacyl-tRNAs, or via frameshifting. Api-mediated pervasive stalling of pre-release ribosomes futilely activates the ribosome rescue systems. Understanding the unique mechanism of Api action in living cells may contribute to development of new treatments for infections and genetic diseases, and research tools for genome exploration.

Introduction

The ribosome is a complex molecular machine which translates mRNA into protein and represents one of the main antibiotic targets in the bacterial cell. Various steps of protein synthesis are inhibited by natural and synthetic antibacterials (Lin et al., 2018; Polikanov et al., 2018; Wilson, 2009). A number of antibiotics impede initiation of translation by preventing mRNA binding or departure of the ribosome from the start codon (Lin et al., 2018; Polikanov et al., 2018; Wilson, 2009). Numerous inhibitors affect translation elongation by interfering with mRNA decoding, peptide bond formation, translocation, or passage of the nascent protein through the exit tunnel (Lin et al., 2018; Polikanov et al., 2018; Vazquez-Laslop and Mankin, 2018; Wilson, 2009). However, there were no known antibiotics that would specifically target the termination step of protein synthesis. It was only recently that apidaecin (Api), an antimicrobial peptide from honeybees (Casteels et al., 1989) was described as the first antibiotic specifically targeting translation termination (Florin et al., 2017).

Api is a 19-amino acid long proline-rich antimicrobial peptide (PrAMP). Various PrAMPs are produced by insects and mammals in order to protect themselves from bacterial infections (Graf and Wilson, 2019; Scocchi et al., 2011). The antimicrobial activity of PrAMPs is based on their ability to bind to the bacterial ribosome and inhibit protein synthesis (Castle et al., 1999; Krizsan et al., 2014; Mardirossian et al., 2014). PrAMPs bind in the vacant nascent peptide exit tunnel of the large ribosomal subunit (Gagnon et al., 2016; Roy et al., 2015; Seefeldt et al., 2016; Seefeldt et al., 2015). Most of the PrAMPs described to date associate with the exit tunnel and invade the peptidyl transferase center (PTC). By blocking the binding of the first elongator aminoacyl-tRNA, these PrAMPs arrest the ribosome at the start codon, thereby preventing transition from the initiation to the elongation phase of translation (Gagnon et al., 2016; Seefeldt et al., 2016).

The action of Api is principally different. Even though Api also binds in the exit tunnel where it closely approaches the PTC, it does not directly occupy the catalytic site. Structural,

kinetic, and biochemical studies carried out with the synthetic peptide Api137 (Berthold et al., 2013) (refer here throughout as Api), and with model substrates showed that Api traps deacyl-tRNA in the P site and release factors 1 or 2 (RF1 or RF2) in the A site, thereby arresting the ribosome at a stop codon. The model that emerged from these in vitro studies (Florin et al., 2017) postulated that Api can bind only after the ribosome has reached the stop codon, associated with RF1/RF2, and released the fully-synthesized protein, because only then the exit tunnel becomes available for Api binding. This model implied that Api specifically targets the post-release ribosome. Strikingly, however, addition of Api to a cell-free translation system could also lead to accumulation of unhydrolyzed peptidyl-tRNA, indicating that Api was also able to interfere with the peptidyl-tRNA hydrolysis that takes place on the ribosome at the stop codon, seemingly acting at a pre-release state (Florin et al., 2017). To accommodate this additional aspect of Api action, the proposed model considered the excess of ribosomes over RF1/RF2 in the cell. Api-mediated trapping of RF1/RF2 on the post-release ribosomes would lead to RFs' depletion which, in turn, would prevent release of the completed proteins on the majority of the ribosomes that would remain stalled at the stop codon of the open reading frames (ORFs) with peptidyl-tRNA bound in the P site. A hypothetical consequence of the RF1/RF2 depletion and ribosome stalling in the pre-release state, would be the occasional misincorporation of an aminoacyl-tRNA at the 'hungry' stop codons. Indeed, treatment of *Escherichia coli* with Api resulted in an increased production of functional β-galactosidase from a *lacZ* gene with a premature stop codon (Florin et al., 2017).

This mechanism of action of Api has been inferred primarily on the bases of in vitro experiments involving a limited number of artificial substrates and reporters. Furthermore, there is a seeming discrepancy regarding the in vitro and in vivo modes of Api action, since translation of a GFP reporter protein was significantly inhibited by Api in bacterial cells, whereas expression of the same reporter in a cell-free system was only marginally affected even at high Api concentrations (Krizsan et al., 2015; Krizsan et al., 2014). Therefore, the consequences of Api

action upon translating ribosomes in the living cell have remained unknown. Would treatment with Api relocate all the ribosomes towards the stop codons? Would Api stall the ribosomes equally efficiently at the stop codons decoded by RF1 (that operates at UAG and UAA codons) or RF2 (which recognizes UGA and UAA codons)? Are there additional effects that become evident only when this PrAMP acts in the living cell?

In order to address these questions and to investigate the genome-wide impact of Api on translation in bacterial cells we used ribosome profiling (Ribo-seq). Our analysis revealed that Api globally inhibits translation termination, albeit with an unexpected diversity of ribosome redistribution patterns across genes. The general arrest of translation at stop codons leads to a pronounced queuing of elongating ribosomes behind the ribosomes occupying stop codons. Treatment of *E. coli* with Api results in dramatic stop codon readthrough that generates proteins with C-terminal extensions. In a likely futile attempt to compensate for the massive increase in populations of stalled ribosomes caused by Api, cells engage and likely overwhelm the ribosome rescue systems that involve the action of tmRNA, as well as of ArfA and ArfB proteins. Our findings show that the unique Api-mediated inhibition of translation termination is influenced by gene specific features and reveal Api as a potent inducer of stop codon bypass genome wide.

Results

Api redistributes ribosomes within mRNAs

In order to assess the global effect of Api on cellular translation we used Ribo-seq, a technique that shows the distribution of translating ribosomes along mRNA's protein-coding segments (Ingolia et al., 2009; Oh et al., 2011). We first optimized the conditions of Api treatment in order to achieve a significant antibiotic effect while minimizing undesirable secondary events. Incubation of *E. coli* (BL21) cultures for 1 min with increasing concentrations of Api resulted in a severe drop in protein synthesis (*Figure 1-figure supplement 1A*). Exposure

to 1.25 μM of Api, which corresponds to the minimal inhibitory concentration (MIC) that prevents cell growth, reduced translation by as much as 75%. Treatment for 2 min with 4x MIC (6.25 μM) curtailed protein synthesis to nearly 10% of the control and extending the treatment to 10 min achieved ~94% inhibition (*Figure 1-figure supplement 1B*). These results confirmed the previous assertion that Api acts as a general inhibitor of bacterial translation (Castle et al., 1999; Krizsan et al., 2014) and guided the selection of the treatment conditions for the subsequent experiments.

We then proceeded to the Ribo-seq experiments in order to obtain an unbiased view of how treatment with Api alters the distribution of translating ribosomes in cellular mRNAs. Exponentially-growing *E. coli* cells were incubated for 5 min with 4x MIC of Api, conditions that led to a nearly complete inhibition of translation (*Figure 1-figure supplement 1B*), and ribosome-protected mRNA fragments (ribosome footprints) were isolated, sequenced, and mapped to the *E. coli* genome (Becker et al., 2013; McGlincy and Ingolia, 2017). Exposure to Api caused a dramatic redistribution of ribosomes along cellular mRNAs. The most commonly observed pattern within individual genes was a gradual buildup of the ribosome density towards the ends of the ORFs, often spilling into the 3'-intergenic regions (*Figure 1A, Source data 1*). In the operons with narrowly spaced genes, the ribosome density was primarily observed at the junctions spanning 3'-terminal codons of the upstream ORF and 5'-proximal codons of the downstream ORF (*Figure 1B*). These effects were drastically different from those observed previously with retapamulin, a specific inhibitor of translation initiation, which generates precise and sharp peaks representing ribosomes occupying start codons (Meydan et al., 2019) (*Figure 1*). In order to mitigate the uncertainty of assigning reads at the junctions of adjacent or overlapping genes in the operons, we limited our subsequent analysis to actively translated genes that are separated by at least 50 nts from the nearest gene (see Materials and Methods). We then carried out a metagene analysis of ribosome coverage near the stop codons (*Figure*

2), which revealed several major effects of Api action that we will discuss in the following sections.

Api acts as a global inhibitor of translation termination

A prominent outcome of Api treatment is a significant (~10-fold) increase of the average normalized ribosome density at stop codons (*Figure 2*). This result reveals Api as a potent global inhibitor of translation termination in bacterial cells and expands the previous findings of the in vitro experiments which showed that Api could arrest ribosomes at the stop codon of several model genes during cell-free translation (Florin et al., 2017).

The extent of the Api-induced increase in stop codon occupancy varied significantly between individual genes. To systematically assess the range of the effects and gain insights into the factors contributing to gene specificity of Api action, we calculated the stop codon (SC) score. The SC score reports the ribosome density within the last three codons of the genes (*i.e.*, the last two sense codons and the stop codon of the ORF) relative to the average density across the entire gene, including the 40 nts of the 3' untranslated region (3'UTR) immediately following the ORF stop codon (*Figure 3A, Figure 3- figure supplement 1*). In the Api-treated cells, the SC scores of the majority of genes shifted to higher values compared to the untreated control, with 25% of the genes exhibiting scores above 16 and 8% genes with the scores exceeding 32, reflecting a dramatic increase in stop codon occupancy (*Figure 3A,B*). In addition, the SC scores in the Api treated cells show a much broader distribution compared to those of the untreated control (mean absolute deviation = 9.3 for the Api sample vs. 1.4 for the control) (*Figure 3B*), indicating that the extent of Api-induced ribosome stalling at stop codons differs widely between individual genes.

One of the factors that could contribute to the gene-specific effects of Api is the stop codon identity, as the UAG and UGA codons are decoded exclusively by RF1 or RF2, respectively, while the UAA codon can be recognized by either one of the two factors. Indeed, within the Api sample, genes ending with the UGA stop codons have a significantly lower

median SC score compared to those with UAA or UAG (*Figure 3B*). This result suggests that either Api traps RF2 less efficiently than RF1, possibly due to a faster RF2 turnover (Florin et al., 2017), or that occupancy of UGA codons by ribosomes is preferentially reduced due to downstream events of Api action (see below). Looking for other features associated with Api-induced stop codon we also noted that the high SC-score ORFs ending with UAA showed a significant enrichment of C and G nucleotides in the first and second positions of the antepenultimate codon, and an increased presence of Gs at the same positions of the last sense codon, possibly reflecting the prevalence of arginine and glycine residues in the respective positions of the nascent protein (*Figure 3C,D*). No remarkable sequence context features were detected for high-SC score genes with UGA stop codon (*Figure 3- figure supplement 2A*). Similarly, none of the other examined properties, including mRNA abundance, its propensity to form stable secondary structures, or the number of ribosomes per mRNA molecule show any strong correlation with the SC scores of the genes in the Api-treated cells (*Figure 3- figure supplement 2B*).

Taken together, our data show that one of the major effects of Api on cellular translation is gene-specific arrest of the ribosomes at stop codons, mainly influenced by the stop codon identity and possibly by specific features of the mRNA sequence, the nature of the nascent protein residing in the terminating ribosome, or the translation dynamics.

Api-induced translation arrest at stop codons results in queuing of the elongating ribosomes

At least three distinct waves of ribosome density are observed in the metagene profile upstream from the stop codons in the Api sample (*Figure 2*). The crests of the waves are spaced by ~27 nts, a distance roughly corresponding to the size of the ribosome-protected mRNA segment (Oh et al., 2011), raising the possibility that this upstream density likely represents elongating ribosomes queued behind the one arrested at the stop codon. The

queued ribosomes occupying inner codons of the ORFs would carry intact nascent polypeptides and should be refractory to Api binding (Florin et al., 2017). We therefore hypothesized that the queued ribosomes could be dissociated from mRNA by the action of puromycin (Pmn), an antibiotic which is known to release the nascent protein from ribosomes whose PTC A site is accessible (Traut and Monro, 1964). Indeed, metagene analysis showed that Pmn treatment of a lysate originated from Api treated cells significantly reduced the amount of queued ribosomes (*Figure 2- figure supplement 1A*). Consistently, because the Api-stalled ribosomes associated with RF1/RF2 should not be susceptible to Pmn, the relative height of ribosomal density peak at the stop codons is significantly increased (*Figure 2- figure supplement 1A*). Yet, the pattern of the ribosome density at individual genes still remained complex (*Figure 2- figure supplement 1B*), suggesting that either some of the ribosomes stalled elsewhere outside of the stop codons are inaccessible to Pmn or that Pmn treatment requires further optimization.

Api treatment leads to pervasive stop codon readthrough

The metagene profile of the Api sample shows a dramatic increase in the number of ribosome footprints mapping to the regions downstream from the stop codons of the well-separated genes (*Figure 2*). Similar to the SC score, we created the readthrough (RT) score, which characterizes the ribosome density at the first 40 nts of the 3'UTR relative to the total ORF-associated density. In the control sample, the RT is very low for most genes because very few ribosomes are found downstream of stop codons. In contrast, in the Api sample >90% of the genes have an RT score greater than 1, indicating higher relative density in the 3'UTR than in the ORF itself due to pervasive and strikingly efficient stop codon bypass (*Figures 4A, Figure 4- figure supplement 1*).

The ribosome footprints in the 3'UTRs could represent post-termination ribosomes that have released the completed protein but failed to dissociate from mRNA and somehow migrated past the stop codon. Alternatively, the 3'UTR footprints may correspond to ribosomes that, while

retaining the fully synthesized protein, bypass the stop codon and continue translation. In order to distinguish between these two possibilities, we first tested whether the 3'UTR-associated ribosomes stalled at stop codons, a scenario that would be compatible with continuation of translation past the main stop codon. Indeed, the metagene analysis shows the peak of the ribosome footprints at the first in-frame downstream stop codon (*Figures 4- figure supplement 2A*), indicating that ribosomes that bypassed the termination signal of the main ORF are actively translating downstream mRNA sequences. We then used shotgun proteomics to test whether exposure of cells to Api leads to productive translation of the non-coding mRNA segments and generation of proteins with C-terminal extensions. To allow for accumulation of proteins synthesized during Api treatment, we exposed cells for 1 h to a sublethal concentration of Api (0.5x MIC) permitting protein synthesis to continue, even if at a reduced level. In addition, we also incubated cells for 1 h with a higher Api concentration (4x MIC). We then analyzed the proteins synthesized in treated and control cells, using custom algorithms to search for tryptic peptides encoded in the 150 nt-long segments downstream from the stop codons of the annotated ORFs (see Materials and Methods). Even when applying strict filtering criteria (Gessulat et al., 2019), we were able to identify a significant number of peptides encoded in the genomic regions downstream from the ORF stop codons in both of the Api samples (*Figure 4B and Source Data 3*). The same analysis found no such peptides in the control sample. The number of identified peptides encoded in the 3'UTRs increased further upon applying a less strict filter (*Figure 4-figure supplement 2B*). These results argued that genome regions downstream of the stop codons of the annotated ORFs are actively translated in the cells exposed to Api. Nearly half (49 %) of the identified 'extension' peptides were encoded in frame with the upstream ORF (*Figure 4C*) and thus, were likely produced by the ribosomes that misread the main ORF stop codon as a sense codon and continued translating the downstream mRNA sequence. Consistently, in the three identified tryptic peptides encoded in mRNA sequences spanning the ORF termination signal, stop codon was mistranslated by a near-

cognate aminoacyl-tRNAs (*Figure 4-figure supplement 3*). Smaller fractions of the identified downstream peptides were encoded in the (-1) or (+1) frames relative to the main ORF (*Figure 4C and Source data 3*). These peptides also likely belong to C-terminal extensions of the main-ORF proteins given that stop codons can be bypassed via frameshifting of the ribosomes stalled at termination sites in the pre-release state, as was observed in the experiments of Gross and coworkers (Baggett et al., 2017). The sample size of the 'extension' peptides was insufficient to systematically identify the mRNA or nascent protein features conducing to the stop codon bypass via frameshifting. However, the presence of a slippery sequence preceding the stop codon (e.g. in *arcB*) (*Figure 4-figure supplement 4A*) or the possibility of repairing of peptidyl-tRNA in a different frame (e.g. in *rplE*) (*Figure 4-figure supplement 4B*) could be among the factors contributing to synthesis of proteins' C-terminal extensions due to ribosome frameshifting. Even though it is possible that presence of C-terminal extensions could lead to undesirable protein interactions, Api treatment did not result in detectable accumulation of protein aggregates in the cells under our experimental conditions (*Figure 4-figure supplement 5*).

Taken together, our results show that stop codon bypass and production of proteins with C-terminal extensions is one of the major consequences of Api action. Translation past the stop codons is likely a consequence of two sequential effects of Api on cellular translation: 1) Binding of Api to the post-release ribosomes at stop codons sequesters the available RF1/RF2 proteins, and 2) Depletion of RF1/RF2 compels the majority of ribosomes to stall at stop codons in a pre-release state with the intact peptidyl-tRNA in the P site - a state conducive to stop codon bypass by amino acid misincorporation or via frameshifting.

Api treatment distorts the cell proteome and activates cellular ribosome rescue systems

Exposure of cells to Api leads to a significant deregulation of the proteome. One of the most prominent effects is an increase in the relative content of ribosomal proteins and other factors related to the function and assembly of ribosomes (*Figure 5-figure supplement 1A and Source Data Y*). Among the top 50 proteins whose abundance is increased in the cells exposed to 0.5x MIC of Api, 19 are related to translation (*Figure 5-figure supplement 1B*). This shift apparently reflects an attempt to compensate for the reduced protein synthesis capacity caused by the Api inhibitory action (*Source Data Y*). Curiously, 13 other proteins among the top 50 are either associated with the inner or outer membrane or reside in the periplasm (*Figure 5-figure supplement 1B*), suggesting a still unknown link between Api action and protein secretion.

Analysis of the Ribo-seq data showed that the highest peak of ribosome occupancy in the Api-treated cells corresponds to the stop codon of the degron-encoding sequence in tmRNA (*Figure 5A,B*). tmRNA is a component of a conserved bacterial system that rescues stalled mRNA-associated ribosomes with an empty A site (Buskirk and Green, 2017; Moore and Sauer, 2005). Following tmRNA binding to the A-site, the ribosome switches templates, synthesizes the tmRNA-encoded degron sequence, and terminates translation at the UAA stop codon (Buskirk and Green, 2017; Moore and Sauer, 2005). tmRNA is known to operate on ribosomes that reach the 3' end of non-stop mRNAs or those stalled due to scarcity of A-site ligand (Ivanova et al., 2004; Janssen et al., 2013; Subramaniam et al., 2014). In the cells treated with Api, both types of substrates are generated. First, the ribosomes stalled at stop codons in a pre-release state due to the shortage of available RF1/RF2, could be potentially recognized by tmRNA as requiring rescue (Li et al., 2007). In addition, Api-stimulated stop codon bypass enables the translating ribosome to reach the 3'-termini of some RNA transcripts (*Figure 5C*), leading to further accumulation of tmRNA-targetable stalled ribosomes. The sharp increase of ribosome occupancy at the tmRNA stop codons (*Figure 5B*) argues in favor of the massive recruitment of tmRNAs to the stalled ribosomes in the Api-treated cells. The Api-mediated extreme increase in tmRNA engagement is not associated with an upshift in its expression (*Source Data Z*) and

thus, must overwhelm the capacity of this mechanism. Consistently, the cell attempts to activate the two other *E. coli* backup rescue factors, ArfA and ArfB (reviewed in (Buskirk and Green, 2017)). For the *arfA* gene in the Api treated cells, we observed a nearly 10-fold increase in the abundance of its transcript and a more than 7-fold higher number of ribosomes associated with its mRNA (*Figure 5D and Source Data Z*). The relative expression of *arfB* transcript increases by ~ 40% and there are ~ 4 times more ribosomes per *arfB* transcript (*Source Data Z*). It is unlikely, however, that either of the ribosome rescue systems can mitigate the consequences of Api action because deletion of tmRNA, *arfA* or *arfB* genes does not increase cell sensitivity to Api (Figure 5-figure supplement 1C).

Api increases start codon occupancy at some genes

While the predominant effect of Api on cellular translation is the build-up of ribosome density in the vicinity of stop codons (Figure 2), a metagene analysis of the 5' ends of genes showed a moderate increase (~ 2-fold) of the number of ribosome footprints at the start codons of the ORFs in the Api sample compared to the control (*Figure 2-figure supplement 2A*). Among the genes with the strongest start codon effects, we selected *zntA*, *srmB*, *cysS*, *tyrS* and *yhbL* to test in vitro whether Api directly delays the ribosome departure from the initiator codon. While translation arrest at stop codons is readily detected by toeprinting analysis at 50 μM of Api (Florin et al., 2017), no start codon effects were observed at this concentration of the inhibitor in any of the tested ORFs. However, increasing Api concentration to 2 mM led to the appearance of a start codon toeprint bands in the *zntA* and *tyrS* templates (*Figure 2-figure supplement 2B-C*), while a similar effect was much weaker or completely absent with the other tested genes. The moderate effect of Api on translation initiation is reminiscent of the main mode of action of other PrAMPs (Gagnon et al., 2016; Roy et al., 2015; Seefeldt et al., 2016; Seefeldt et al., 2015) and could be explained by its ability to bind with a reduced affinity to the ribosome even in the absence of RF1/RF2 (Florin et al., 2017; Kolano et al., 2020; Krizsan et al., 2014). However, it

remains to be elucidated whether the mechanism of the weak inhibition of translation initiation by Api is comparable to that of other PrAMPs.

Discussion

In this paper, we analyzed the impact of the antibacterial peptide Api on translation in the living cell. Our findings expanded the insights obtained in our previous biochemical experiments and structural analysis and illuminated new aspects of Api action that could be uncovered only by in vivo approaches. The Ribo-seq and proteomics studies revealed the complex nature of Api effects, where the immediate action of the antibiotic, trapping of RFs on post-release ribosomes, then triggers multifaceted downstream events leading to the dramatic alteration of ribosome behavior in the vicinity of stop codons of the mRNA ORFs.

One of the main effects of Api in the bacterial cell is the arrest of translation at the end of the protein coding sequences revealed by Ribo-seq as a significantly increased density of ribosome footprints at the stop codons. According to the previously suggested model (Florin et al., 2017), two different populations of ribosomes account for the dramatic increase of the stop codon occupancy. A fraction of ribosomes, arrested in the post-release state due to the direct Api action, likely carries deacylated tRNA in the P-site, RF1 or RF2 in the A site, and Api bound in the nascent peptide exit tunnel. However, this fraction is expected to be a minor contributor of stop codon footprints because in exponentially growing *E. coli* cells, ribosomes outnumber RF molecules by one to two orders of magnitude (Bremer and Dennis, 1996; Li et al., 2014; Schmidt et al., 2016). Sequestering RFs in these post-release complexes would prevent peptidyl-tRNA hydrolysis on the rest of the ribosomes that reach the end of an ORF. Thus, in cells treated with Api, the majority of ribosomes paused at the stop codons are likely those stalled in a pre-release state, with an intact peptidyl-tRNA in the P site and an empty A site.

Ribo-seq analysis revealed that the extent of Api-induced ribosome arrest differs significantly in its magnitude between genes. One of the factors that influences the gene-

specificity of Api action is the stop codon identity: arrest at the RF2-specific UGA codons was significantly less pronounced than that at the UAA or UAG stop codons (*Figure 3B*). Several scenarios may account for this effect. The ribosome-tRNA-RF2-Api complex could be less stable than the equivalent complex with RF1 (Florin et al., 2017) and may linger for a shorter time at the stop codon prior to its dissociation. Another possibility derives from the fact that the only time window for Api to stably associate with the post-release ribosome is after the completed nascent protein has vacated the exit tunnel, but before RF1 or RF2 have dissociated. If the residence time of RF2 on the post-release ribosome is shorter than that of RF1, which is a distinct possibility since RF2 can disengage spontaneously while RF1 dissociation requires binding of the RF3 GTPase (Adio et al., 2018), ribosomes would be less frequently trapped by Api at UGA codons. An additional factor that may affect the Api-induced termination arrest is the efficiency of stop codon bypass, which is known to be higher for pre-release state ribosomes paused at UGA than for those at UAG or UAA codons (Tate et al., 1999).

The stop codon identity does not account for the entire range of gene-specific effects of Api on termination because the SC scores differ dramatically even between genes ending with the same stop codon (*Figure 3B*). Neither mRNA abundance or folding propensity, nor the number of ribosomes loaded onto mRNA seem to define the gene-specific action of Api (*Figure 3-figure supplement 2B*), indicating that other factors, that remain to be elucidated, might be at play. The more frequent appearance of C-terminal glycine and/or antepenultimate arginine in the proteins encoded in UAA-ending genes with a higher SC score (*Figure 3C*) could be a manifestation of nascent protein effects on some aspects of Api action yet to be explored. Noteworthy, the presence of arginine in the third to last amino acid position of the nascent peptide was shown to correlate with enhanced termination (and concomitant reduced readthrough frequency) at UGA codons in *E. coli* (Mottagui-Tabar et al., 1994; Parker, 1989).

Direct or indirect Api-induced ribosome stalling at stop codons causes severe ribosome queuing. Even though collisions of a trailing ribosome into a stalled one have been observed in

bacteria and eukaryotes exposed to translation elongation inhibitors (Kearse et al., 2019; Mohammad et al., 2019), the extent of ribosome queuing in the Api-treated cells appears to be especially pronounced. The impressive ability of Api to cause queuing likely stems from the unique mechanism of its action. In contrast to elongation inhibitors which can simultaneously arrest ribosomes at many codons within the gene, Api preferentially arrests translation at a single site, the stop codon; all the trailing ribosomes on the same mRNA continue translation until they run into the traffic jam caused by the termination site roadblock. The pronounced ribosome queuing in the Api-treated cells illustrates a distinctive feature of a translation termination inhibitor as an antimicrobial: Api needs to bind to only a few terminating ribosomes in order to preclude a much larger number of inhibitor-free ribosomes from participating in translation. Api-induced ribosome queuing parallels the appearance of a second 'shadow' peak of ribosome footprints behind the slowly terminating ribosomes in *E. coli* cells devoid of RF3 (Baggett et al., 2017). However, queuing in the Api-treated cells is significantly more pronounced than in the ΔRF3 cells. Piling-up of the translating ribosomes behind the slowly terminating one has been also observed in eukaryotic cells (Kasari et al., 2019). Structural analysis of queued ribosomes suggest that they can stall in a partially rotated state prior to completing translocation (Juszkiewicz et al., 2018; Matsuo et al., 2020). We noted, however, that addition of Pmn to the lysates prepared from Api-treated cells significantly reduced queuing (*Figure 2-figure supplement 1*), suggesting that in a large fraction of the queued ribosomes the A site is accessible for Pmn binding.

Our Ribo-seq experiments additionally revealed a striking and pervasive Api-induced genome-wide stop codon readthrough resulting in an abundance of ribosome footprints downstream of ~ 90% of the genes that we analyzed. When a similar phenomenon was observed in eukaryotic cells, the three-nucleotide codon periodicity of the downstream ribosome footprints was used as the distinct signature of actively translating ribosomes (Dunn et al., 2013; Wangen and Green, 2020; Young et al., 2015). The less precise ribosome assignment in

bacterial Ribo-seq data and sequence bias of MNase action (Baggett et al., 2017; Hwang and Buskirk, 2017; Mohammad et al., 2019) makes such analysis poorly applicable for assessing the translation status of 3'UTR-associated ribosomes in the Api sample. Nevertheless, the appearance of peptides encoded in the downstream mRNA sequences, revealed by shotgun proteomics, and the increased ribosome occupancy of the downstream stop codons strongly argue that in the Api-treated cells a significant fraction of translating ribosome translate past the end of the ORFs and synthesize proteins with C-terminal extensions. Some level of stop codon readthrough can be also induced by other ribosome-targeting antibiotics, such as aminoglycosides, negamycin and others (Olivier et al., 2014; Polikanov et al., 2014; Thompson et al., 2004; Wangen and Green, 2020). However, Api's ability to stimulate bypass is exceedingly robust, leading to appearance of ribosome footprints downstream of not only the first, but also of the subsequent stop codons (*Figure 5B*). Because Api does not inhibit translation elongation (in contrast to the above mentioned readthrough-inducing antibiotics (Cabanas et al., 1978; Polikanov et al., 2014; Wang et al., 2012)), more ribosomes can reach the end of the ORFs in the Api-treated cells, thereby triggering a higher rate of stop codon readthrough. Additionally, unlike miscoding antibiotics, Api does not reduce the general accuracy of translation and thus, an Api-like mechanism could be exploited for medical applications where premature stop codon readthrough is required (Huang et al., 2019; Keeling et al., 2014).

Although we cannot exclude a possibility that some of the extension peptides identified by proteomics result from re-initiation of translation after protein release at the main ORF stop codon (Young et al., 2015), we favor the scenario that most of the ribosome footprints found downstream of the main ORF belong to the ribosomes synthesizing C-terminally-extended protein. One of the arguments in favor of this view is that nearly half of the extension peptides identified by the proteomics analysis are encoded in 0-frame relative to the main ORF. This observation also argues that the most prevalent mechanism of Api-mediated stop codon

readthrough is misincorporation of an amino acid when the stop codon is positioned in the A-site of the pre-release ribosome. Analysis of the few identified tryptic peptides that result from erroneous decoding of stop codons showed that amino acid misincorporation during readthrough is commonly driven by a near-cognate aminoacyl-tRNAs (*Figure 4-figure supplement 3*). The appearance of out-of-frame extension peptides in the Api-treated cells shows that Api-induced stalling of pre-release ribosomes at the stop codons can also occasionally lead to stop codon bypass via frameshifting. Even though with some genes the putative mechanisms of frameshifting could be envisioned (*Figure 4-figure supplement 4*), many other scenarios could be potentially involved (Ma et al., 2018).

Conceivably, acquisition of an unwanted C-terminal extension may interfere with the protein stability or its propensity for aggregation. Nonetheless, under our Api treatment conditions, we did not detect any significant accumulation of protein aggregates (*Figure 4-figure supplement 5).* It remains possible, however, that synthesis of proteins with C-terminal extensions could contribute to the antimicrobial activity of Api since these aberrant appendices may negatively affect the proteins' catalytic capacity, ligand binding ability, or interactions with other proteins.

In spite of the pervasive nature of Api-induced stop codon bypass revealed by Ribo-seq, our proteomics analysis identified only a limited number of peptides corresponding to the C-terminal protein extensions. This is probably not surprising, because in our experimental setup, the Api-treated cells not only had a fairly limited time (1 h) to synthesize extended proteins, but were doing so under conditions of diminished translation. Other possible confounding factors include the use of only trypsin digest and the fact that the C-terminal extensions are generally much shorter than the main-frame proteins and thus can yield only few potentially detectable peptides. Optimization of the Api-treatment conditions and increasing the depth of the proteomics analysis would likely help to identify more of the C-terminally-extended proteins. Importantly, when applying strict filtering criteria, the extension peptides were only detected in

the Api-treated cells (*Figure 4B*). Because the mechanisms of Api-induced stop codon bypass should be similar to those operating in the untreated bacteria, Api could be instrumental in elucidating fundamental features of spontaneous stop codon readthrough that operate in bacterial cells (Baggett et al., 2017; Ma et al., 2018).

By prompting the translating ribosomes to stall in a pre-release state at the stop codons and by allowing translation to incidentally proceed up to the 3' ends of mRNA transcripts (*Figure 5C*), Api triggers the activation of the ribosome rescue systems. This is manifested as a dramatic increase in the ribosome occupancy of the stop codon of the tmRNA ORF and in the transcriptional and translational upregulation of the *arfA* and *arfB* genes. However, in the cells exposed to Api, the rescue systems are likely worthless. tmRNA-mediated rescue of stalled ribosomes relies on translation termination at the UAA codons of the degron ORF in tmRNA (reviewed in (Buskirk and Green, 2017)). Yet, the lack of available RF1/RF2 in the Api-treated cells would prevent the release of the degron-tagged protein, and the ribosome, previously stalled at the hungry stop codon of a cellular ORF or at the mRNA 3' end, would now instead become arrested at the tmRNA ORF termination site and thus, remain unproductive. Depletion of the available tmRNA pool, leads to activation of the backup rescue systems which should be also ineffectual in the Api-treated cells. ArfA facilitates translation termination at non-stop mRNAs by binding to the empty A site of the ribosomal small subunit and promoting binding of RF2 which can then release the stalled protein. Once again, the lack of available RF2 in the Api-treated cells should prevent ArfA from carrying out its rescue mission. An indication of the futility of the ArfA-based rescue system is the appearance of an exceedingly high ribosome density peak at the end of the non-stop *arfA* mRNA (*Figure 5D*), where the stalled ribosomes are expected to be released by the action of the ArfA protein itself (Garza-Sanchez et al., 2011). Consistently, proteomics analysis did not show any significant increase in the relative abundance of ArfA in the cells exposed to Api (*Source Data X*). Despite acting independently from the primary RFs, a third rescue system that involves the peptidyl-tRNA hydrolysis activity

of the alternative RF, ArfB, should be also futile. Mimicking RF1/RF2, ArfB contains the conserved GGQ motif which reaches into the PTC active site (Gagnon et al., 2012). Therefore, it is highly likely that Api can trap ArfB in the post-release ribosome and deplete its available pool. Thus, it appears that none of the known means that the bacterial cell normally exploits for salvaging stalled ribosomes would be of much use when translation is inhibited by Api. In agreement with this notion, inactivation of any of the rescue systems does not sensitize *E. coli* to the Api action (*Figure 5-figure supplement 1C*).

One of the unexpected aspects of Api action revealed by in vivo studies is increased start codon occupancy in some genes. The low affinity of Api for the vacant ribosome (Florin et al., 2017; Kolano et al., 2020; Krizsan et al., 2014) could potentially account for association of the antibiotic with the initiating ribosome and either block the first peptide bond formation by displacing the fMet moiety of the initiator tRNA in the P site, or by interfering with the first act of translocation. Because the start codon effects could be observed in vitro only at very high concentrations of Api (*Figure 2-figure supplement 2B-C*), the in vivo effects could either involve additional factors absent in the cell-free translation system or may reflect secondary downstream aspects of Api action.

Understanding the mode of Api action in the bacterial cell helps to rationalize the seeming discrepancy between its in vivo and in vitro effect on translation, where it readily inhibits cellular protein synthesis, but only marginally reduces expression of reporter proteins in cell-free systems (Castle et al., 1999; Krizsan et al., 2015; Krizsan et al., 2014). In cells exposed to Api, stalling of post- and pre-release ribosomes at stop codons of multiple ORFs, queuing of Api-free ribosomes in a translation-incompetent state, and depletion of available RFs, leads to a rapid cessation of protein synthesis. In contrast, in cell-free systems, where only one type of mRNA is present and all the available RFs are used for the release of the reporter protein, many mRNA molecules will be translated at least once prior to depletion of the RF pool resulting in poor reporter inhibition.

While the value of antibiotics as critical medicines is obvious, they can be also used as discovery tools for research. Using the translation initiation inhibitor, retapamulin, in combination with Ribo-seq we developed previously the Ribo-RET approach for identifying translation start sites in bacteria, revealing a universe of hidden protein-coding sequences (Meydan et al., 2019). Many of the newly identified alternative ORFs within the annotated genes or ORFs located in the intergenic regions, encode short proteins that are functionally involved in cell physiology, whereas translation of others may play important regulatory roles (Meydan et al., 2019; Weaver et al., 2019). Ribo-seq, enhanced by the use of a translation termination inhibitor, can bolster further our ability to detect the translated sequences encoded in the genomes. Because Api action results not only in translation arrest at the stop codons, but also in ribosome queuing and stop codon readthrough (*Figure 2*), its immediate application for mapping translation termination sites could be challenging. Nevertheless, with additional manipulations, e.g. Pmn treatment to remove queued elongating ribosomes (*Figure 2-figure supplement 1*), and with the proper bioinformatics analysis, Api and other similar inhibitors could be repurposed for genome-wide analysis of stop codons of protein-coding regions. The combined use of translation initiation and termination inhibitors together with Ribo-seq could provide new insights in the principles of genetic encoding and regulation of gene expression.

Materials and Methods

Reagents

Api137 (Berthold et al., 2013), which we refer to simply as Api, was synthesized by NovoPro Biosciences Inc. DNA oligonucleotides were synthesized by Integrated DNA Technologies.

Protein synthesis inhibition assay

Inhibition of cellular protein synthesis by Api was analyzed by metabolic labeling as described previously (Meydan et al., 2019) with the following modifications. *E. coli* BL21 Δ*tolC* cells (Table 1) were grown overnight in MOPS medium (Teknova) lacking methionine (MOPSΔMet). Cells were diluted 1:200 into fresh MOPS-Met and grown at 37°C until the culture reached a density of A_{660} of 0.2. Aliquots of the exponentially growing cells were added to tubes containing appropriately diluted Api in MOPSΔMet medium to obtain 0.75, 1.5, 3.1, 6.25, 12.5, 25 and 50 μM as final Api concentrations in the total volume of 100 μL. After 2 min incubation, 28 μL were transferred to another tube containing 2 μL MOPSΔMet medium supplemented with 0.3 μCi of L-[^{35}S]-methionine (specific activity 1,175 Ci/mmol) (MP Biomedicals). Following 90 s incubation, the content was transferred onto Whatman 3MM paper discs pre-wetted with 5% TCA and the procedure was continued as described previously (Meydan et al., 2019).

The time course of protein synthesis inhibition was performed as described above, except that Api was directly added to a final concentration of 6.25 μM to the exponentially growing culture in MOPSΔMet medium and aliquots were taken at 0, 2, 5 and 10 min.

Cell growth and cell lysates preparation for Ribo-seq experiments

The Ribo-seq experiments were performed as described previously (Meydan et al., 2020; Meydan et al., 2019) using cells grown in MOPS medium. Briefly, the overnight cultures of *E. coli* BL21 Δ*tolC* cells (Table 1) were diluted 1:200 in 150 mL of medium and grown at 37°C in flasks until reaching density of A_{600} ~ 0.4. For Api-samples, 4.12 mg of dry Api powder was added directly to the cultures to a final concentration of 12 μM and incubation with shaking continued for 5 min. Untreated (control) and Api-treated cells were harvested by rapid filtration, flash frozen in liquid nitrogen and cryo-lysed in 650 μL lysis buffer (20 mM Tris pH 8.0, 10 mM $MgCl_2$, 100 mM NH_4CL, 5 mM $CaCl_2$, 0.4 % Triton-X100, 0.1% NP-40) supplemented with 65 U RNase-free DNase I (Roche) and 208 U Superase•In™ RNase inhibitor (Invitrogen). The pulverized cells were thawed at 30°C for 2 min and incubated in an ice water bath for 20 min and lysates were clarifyied by centrifugation at 20,000 x g for 10 min at 4°C. One aliquot of the clarified lysates was preserved frozen for RNA-seq analysis, another aliquot was immediately treated with MNase (se below); the third aliquot was treated by puromycin (Pmn) as follows. The cell lysates were supplemented with 1 mM Pmn (Millipore-Sigma), 10 mM creatine phosphate (Millipore-Sigma) and 40 μg/mL creatine kinase (Roche), and incubated for 10 min at 25°C with shaking at 1400 rpm. Cell lysates, treated or not with Pmn, were subjected to MNase treatment by adding 450 U MNase (Roche) per 25 A_{260} units of lysate, 3 mM GMPPNP and incubating for 60 min at 25ºC. The MNase reaction was quenched by addition of EGTA (5 mM final concentration). Following sucrose gradient centrifugation and collection of the 70S ribosome peak (Becker et al., 2013), subsequent solation of ribosomal footprints from the and libraries preparation were performed as described (McGlincy and Ingolia, 2017).

Processing of ribosome footprints for Ribo-seq analysis

The Ribo-seq reads were de-multiplexed using Cutadapt (Martin, 2011) as described (Aleksashin et al., 2019). The 2 random nts at the 5' end and 5 nts at the 3' end of the reads, added during the Ribo-seq library preparation (McGlincy and Ingolia, 2017; Meydan et al.,

2020), were trimmed and then the GALAXY pipeline was used to process and align the reads to the reference BL21 genome (GenBank ID CP001509.3) (Meydan et al., 2020; Meydan et al., 2019). The 26 to 39 nt-long reads were used in the subsequent analyses with the first position of the P-site codon assigned 16 nt from the 3' end of the read (Mohammad et al., 2019).

Metagene analysis

The metagene analyses at the annotated 3' and 5' regions followed the previously described protocol (Aleksashin et al., 2019). For the inclusion in the analysis, the well-separated ORFs had to satisfy three criteria in all four datasets (two control and two Api-treated biological replicates): i) The ORF length is at least 300 nt, ii) at least 5% of the positions within the coding sequence had assigned reads values above zero, and iii) the average number of rpm per nt in an ORF is ≥ 0.005. Ribosome footprint density at each nucleotide was normalized to the average coverage of the entire ORF plus 100 nts up- and downstream. The mean of the normalized values was calculated and plotted for the regions around the start and stop codons of the ORF

The metagene analysis of the first in-frame stop codons of the downstream regions was carried out using 3769 genes with such codons present within the 225 nucleotides downstream of the annotated ORF. Normalized read coverage, calculated for each nucleotide within a 200 nt window centered around the last nucleotide of the downstream stop codons, was determined by dividing ribosome footprint coverage at each position by the maximum coverage value within the window. Normalized coverage was then summed for each position in the windows and plotted.

Calculation of stop codon- and readthrough scores

The well-separated genes included in the analysis were required to meet two criteria in all four datasets (two control and two Api-treated biological replicates): i) they were separated from the upstream and downstream adjacent genes by at least 50 nts, and ii) they have a

coverage density of at least 0.05 reads per nt in the protein-coding sequence, excluding the first and last 9 nts of the ORF. Because in the Api samples a large fraction of ribosome footprints was found in the downstream region likely representing the ribosomes that have translated the upstream ORF, the region considered as 'total' for each gene was assigned as starting from 1 nt before the start codon to 40 nt after the stop codon. The stop codon (SC) region was assigned as nine 3'-terminal nt of the ORF (the last two sense codons and the stop codon); the readthrough (RT) region encompassed 40 nt downstream from the ORF stop codon. The SC and RT scores were calculated by dividing the average ribosome density within the SC region or the RT region, respectively, by the total average density. The mean SC and RT scores of each gene were used in further analyses.

RNA-seq analysis

Aliquots of the clarified cell lysates from the samples prepared to Ribo-seq analysis (see above) were used to extract and analyze total RNA as previously described (Aleksashin et al., 2019). Briefly, total RNA was purified by acidic phenol extraction, short RNAs and rRNA were subtracted using the MEGAclear (Ambion) and MicrobEXPRESS (Ambion) kits, respectively, mRNA was fragmented via alkaline fragmentation and, after size-fractionation and isolating fragment sin the 15-45 nt range, converted to the library for next generation sequencing.

The RNA-seq analysis was performed as previously described (Aleksashin et al., 2019). Briefly, Cutadapt was used to process and demultiplex the reads. Kallisto (v.0.44) (Bray et al., 2016) and Sleuth (v.0.30) (Pimentel et al., 2017) were used to align the reads and perform a differential expression analysis, respectively. To align reads to the *ssrA* transcript, the GALAXY pipeline was used for alignment and quantifying reads per million after filtering out reads aligning to the non-coding RNA.

Sample preparation for proteomics analysis

All protein preparation steps were performed on ice. The cell pellet from each sample was resuspended in 2 ml TNI lysis buffer (50 mM Tris-HCl, pH 7.5, 250 mM NaCl, 0.5% Igepal CA-630, 1 mM EDTA and 1 complete ULTRA EDTA-free Protease Inhibitor cocktail tablet), sonicated using a probe sonicator (Branson, CT) at 30% power at 55 kHz repeatedly for 20 s with 10 s interval to cool down the lysate until sufficiently clear lysate was obtained. The lysate was then clarified by centrifuging for 20 min at 13,000 g at 4 °C in order to remove cell debris. The cleared supernatant was transferred to a fresh tube and total protein was precipitated by addition of $CHCl_3$/MeOH as previously described (Gao, 2019). Air-dried total protein pellet from each sample was dissolved in 100 mM Tris-HCl pH 8.5, 8 M urea. Protein concentration was measured by BCA protein assay kit (Thermo Fisher). One hundred µg of protein from each sample were digested with trypsin (Promega) at 37°C for 24 hours with an enzyme to protein ratio 1:100 (w/w). After addition of 96% formic acid to the final concentration of 5%, samples were briefly centrifuged at 13,000 g and peptide-containing supernatant was used for further analysis Peptides were fractionated into eight fractions using High-pH Reversed-Phase Peptide Fractionation Kit (Thermo Fisher). Peptide fractions were dried in SpeedVac (Eppendorf, Germany) and resuspended in 20 µl of 0.1% formic acid.

Mass spectrometry analysis

Individual fractions of the tryptic peptides were separated by a capillary C18 reverse phase column of the mass-spectrometer-linked Ultimate 3000 HPLC system (Thermo Fisher) using a 90 min gradient (5%- 85% acetonitrile in water) at 300 nl/min flow. Mass spectrometry data were acquired by an Orbitrap QExactive HF system (Thermo Fisher) with nanospray ESI source using data-dependent acquisition. Raw data were collected and processed by ProLuCID search engine (Xu et al., 2015) and in-house pipeline.

Mass-spectrometry data analysis

Raw files were converted into MSn files using in-house converter or mzml files using MSconvert (Chambers et al., 2012) and then searched by both ProluCID (Xu et al., 2015) and MSFragger (Kong et al., 2017) using standard and extended reference proteomes (see below). The identified peptide sequences were first mapped to the in silico-generated extended proteome, then cross referenced to the standard reference proteome (Uniprot *E. coli* BL21 reference proteome downloaded 2/20/2020). The 'extension' peptides were identified by subtracting all the peptides found in standard reference proteome from the peptides found in the extended proteome. All peptides mapped to the 150 nt-long genomic regions downstream of the stop codons of each annotated ORF and those covering both the tail of annotated ORFs and head of the downstream of the stop codons were reported. All scripts processing the data were written in Python 3.7 and are available at [http://git.pepchem.org/gaolab/api_ribo_ext].

The standard reference proteome was constructed using the annotated reference genome of *E. coli*, strain BL21 DE3 (NCBI GenBank: CP001509.3). Extended reference proteome was generated by amending standard reference proteome with the proteome that could be encoded in three frames in the 150 nt-long genomic regions downstream of the stop codons of the 2100 highly expressed annotated genes (> 112 sequence counts or 17.2 RPMs, the median of all genes, in the Ribo-seq dataset) in the Api-treated sample. The bypass of the first downstream stop codon was presumed to take place in 0/(+1)/(-1) frame using the rules described above for the primary stop codon. The subsequent downstream stop codons were presumed to be translated in 0 frame.

To investigate readthrough pattern of the primary stop codon, another custom proteome database was constructed with the primary stop codon translated into each of the 20 natural amino acids. The mass spectrometry data were then re-processed the same way as described above except using this new extended database.

To elucidate the changes in the proteome among different conditions, all the proteins identified from the above-mentioned search, regardless of the extension status, were quantified using semi-quantitative label-free quantitation method using normalized spectral abundance factor (NSAF) to represent the relative expression level of each protein (Zybailov et al., 2005). All the low confident proteins, i.e. proteins with < 5 spectral counts, were removed from the analysis. The rest of the proteins were compared using NSAF ratio between two conditions and sorted using a gamma distribution cumulative distribution function (*Figure 5-figure supplement 3*). The top 50 genes chosen from each comparison were used as input for pathway analysis using String-DB (Szklarczyk et al., 2019). A heat map of all the protein expression levels across all conditions were generated using NSAFs (*Figure 5-figure supplement 1A*). Genes and conditions were both clustered using hierarchical k-mean clustering algorithm (Gao et al., 2019). The color represents the relative expression level (NSAFs) of each protein quantified as mentioned above.

Toeprinting assay

DNA templates for toeprinting containing T7 promoter and an annealing site for the toeprinting primer were generated via PCR by amplifying the corresponding gene sequences from the *E. coli* BL21 genomic DNA. The following DNA primers were used for preparing the respective gene templates: *zntA* (TAATACGACTCACTATAGGGAAACTTAACCGGAGGATGCCATGTCG and GGTTATAATGAATTTTGCTTATTAACTTTGAACGCAGCAAATTGAGGGGC), tyrS (TAATACGACTCACTATAGGGTTATATACATGGAGATTTTGATGGCAAGC and GGTTATAATGAATTTTGCTTATTAACGACTGGGCTACCAGCCCCCG), *srmB* (TAATACGACTCACTATAGGGGCCCCACACAGAGGTAGAACATGACTGTAACG and GGTTATAATGAATTTTGCTTATTAACGGCTTCCAGCAGGCTTTCGTCG), *ybhL*

(TAATACGACTCACTATAGGGTATATCTTCAGGAGATCGTCATGGACAGATTCC and GGTTATAATGAATTTTGCTTATTAACGATTGCAAGCCAGCCCGGGGTTGTACG), cysS (TAATACGACTCACTATAGGGATGTCTAAACGGAATCTTCGATGCTAAAAATCTTC and GGTTATAATGAATTTTGCTTATTAACTGAATAGGCTTAAATTCCTCTTTTTGGCG). The toeprinting assay was performed as previously described (Orelle et al., 2013) using the PURExpress system (New England Biolabs). When needed, Api was added to the final concentration of 50 μM or 2 mM. The final concentration of edeine was 50 μM. Following 10 min of translation, reverse transcription was carried out for 10 min using toeprinting primer NV1 GGTTATAATGAATTTTGCTTATTAAC (Vazquez-Laslop et al., 2008). Reverse transcription products were separated on a 6% sequencing gel. The gel was dried, exposed to a phosphorimager screen, and visualized in a Typhoon phosphorimager (GE Healthcare).

Aggregation assay

E. coli BL21Δ*tolC* cells were grown in MOPS media to a density of A_{600} ~ 0.4 and then treated for 30 min with 2x MIC of either Api (1.56 μM), spectinomycin (60 μg/mL), or streptomycin (1μg/mL). Control antibiotic treatment conditions were those affording maximum protein aggregation (Ling et al., 2012). Cells were lysed and protein aggregates were isolated as previously described (Tomoyasu et al., 2001). The aggregates were separated with SDS-PAGE and visualized by silver staining.

Acknowledgements

We thank Dr. Mo Hu (Northwestern University Feinberg School of Medicine) for help with statistics modeling analysis of the proteomics data and members of Mankin/Vàzquez-Laslop and Polikanov labs for discussion. This work was supported by the grant from the National Science Foundation (to N.V.-L and A.S.M.) MCB 1951405, and the grant from the National Institutes of Health R35 GM133416 (to Y.G.).

Data availability

Ribo-seq and RNA-seq data have been deposited in the NCBI Gene Expression Omnibus (GEO) database under accession code XXX. Proteomics data have been submitted to the EMBL-EBI Proteomics Identification database PRIDE under accession code XXX.

Figure legends

Figure 1. Api redistributes ribosomes towards the ends of mRNA ORFs. **(A**) Comparison of ribosome footprint density in the *tktA* and *dptA* ORFs in untreated *E. coli* cells with that in cells treated with either Api or the translation initiation inhibitor retapamulin (Ret). (**B**) Ribosome footprint density within genes of the *his* operon in cells treated with no antibiotic, Api or Ret. The Ret Ribo-seq data are from (Meydan et al., 2019).

Figure supplement 1. Api inhibits global protein synthesis in *E. coli* cells.

Source data 1. Source data from ribosome profiling analysis.

Figure 2. Translating ribosomes in cells treated with Api accumulate near stop codons. Metagene plot of the average normalized ribosome occupancy near the annotated stop codons of genes in cells treated (orange) or not (grey) with Api. The solid line indicates the mean value and the shadow plot reflects the standard error between two independent biological replicates. The metagene plot is based on 836 well separated and actively translated genes separated by ≥50 nt. The cartoon illustrates ribosomes stalled at the stop codon in the post- or pre-release state, ribosomes queued upstream from those stalled at termination sites, and ribosomes present in mRNA regions downstream from the main ORF stop codon (readthrough).

Source data 1. Source data from ribosome profiling analysis.

Figure supplement 1. Puromycin reduces the complexity of the Api-mediated ribosomal distribution patterns.

Figure supplement 2. Api moderately increases ribosome density at start codons.

Figure 3. Api arrests ribosomes at translation termination sites. **(A**) *Top*: Stop codon (SC) score was calculated for actively translated genes separated by ≥50 nt as the ratio of ribosome density near the stop codon ('SC', orange rectangle) to the ribosome density within the entire coding and the immediate downstream regions ('Total', light blue rectangle) (see

Materials and Methods for details). *Bottom*: histogram of the SC scores of genes from cells treated (orange) or not (gray) with Api. (**B**) Box plots of SC scores associated with individual stop codons in cells treated or not with Api. Outliers were removed and whiskers span to the min and max remaining values. Two-sided Mann-Whitney *U* tests were performed to assess the significance of difference between genes grouped by stop codons: * $p < 0.05$, **** $p<0.0001$. (**C**) and (**D**) pLogo analyses of nucleotide (**C**) or amino acid (**D**) sequence bias around the termination regions of the top 50% SC-scoring vs. the bottom 50% SC-scoring genes with UAA stop codon from Api treated cells.

Source data 2. SC score correlations.

Figure supplement 1. Comparison of stop codon (SC) scores of each gene in biological replicates.

Figure supplement 2. Evaluation of cellular factors that could contribute to Api-mediated ribosome arrest at stop codons.

Figure 4. Api leads to stop codon bypass and generation of proteins with unintended C-terminal extensions. **(A)** *Top*: Readthrough (RT) score was calculated for actively translated genes separated by ≥50 nt as the ratio of ribosome density within the 40 nts downstream from the stop codon ('RT', orange rectangle) to the ribosome density within the entire coding and downstream regions ('Total', light blue rectangle). *Bottom*: histogram of the RT scores of genes from cells treated (orange) or not (gray) with Api. (**B**) The number of proteins with C-terminal extensions, peptides belonging to the C-terminal extensions of proteins, and peptide-spectrum matches (PSMs) identified by mass-spectrometry in cells treated with 0.5x MIC (light orange bars) or 4x MIC (orange bars) of Api. With the same data-filtering criteria, no such products were detected in the control cells. (**C**) The fraction of identified peptides belonging to C-terminal extensions of proteins in Api-treated cells generated via bypassing the stop codon of the main

ORF by amino acid misincorporation (0-frame), or as a result of -1 or +1 ribosomal frameshifting (fs).

Source data 3. Peptides encoded in the downstream mRNA regions found by proteomics.

Figure supplement 1. Comparison of readthrough (RT) scores of each gene in biological replicates.

Figure supplement 2. In the Api-treated cells, ribosomes actively translate mRNA segments downstream from the stop codon of the main ORF.

Figure supplement 3. Stop codon bypass by near-cognate amino acyl-tRNA misincorporation

Figure supplement 4. Possible scenarios for stop codon bypass via frameshifting in Api-treated cells**.**

Figure supplement 5. Protein aggregation in Api treated cells is not detectable.

Figure 5. Alteration of the proteome and activation of the ribosome rescue systems in response to Api. (**A**) Density of ribosome footprints throughout the *E. coli* genome in cells treated or not with Api. (**B**) Density of ribosomal footprints at the termination region of the tmRNA ORF encoding the degron tag. The position of the main stop codon and two in-frame downstream stop codons of the tmRNA are indicated with red triangles. (**C**) Ribosome footprints near the 3'-ends of the *rpmF* and *infA* transcripts in Api-treated cells. The RNA-seq density is shown below. (**D**) Density of ribosome footprints in the *arfA* gene in Api-treated or control cells. The gray triangle marks the position of the RNase III cleavage site involved in the tmRNA- and ArfA-dependent regulation of *arfA* expression.

Source data 1. Source data from ribosome profiling analysis.

Source data 4. Protein abundance in the untreated and Api-exposed cells.

Source data 5. RNA-seq gene scores.

Source data 6. Ribo-seq gene scores.

Figure supplement 1. Api induced changes in protein abundance

Figure supplement 2. Sensitivity towards Api of cells lacking ribosome rescue systems

References

Adio, S., Sharma, H., Senyushkina, T., Karki, P., Maracci, C., Wohlgemuth, I., Holtkamp, W., Peske, F., and Rodnina, M.V. (2018). Dynamics of ribosomes and release factors during translation termination in *E. coli*. eLife *7*, e34252.

Aleksashin, N.A., Leppik, M., Hockenberry, A.J., Klepacki, D., Vazquez-Laslop, N., Jewett, M.C., Remme, J., and Mankin, A.S. (2019). Assembly and functionality of the ribosome with tethered subunits. Nat. Commun. *10*, 930.

Baggett, N.E., Zhang, Y., and Gross, C.A. (2017). Global analysis of translation termination in *E. coli*. PLoS Genet. *13*, e1006676.

Becker, A.H., Oh, E., Weissman, J.S., Kramer, G., and Bukau, B. (2013). Selective ribosome profiling as a tool for studying the interaction of chaperones and targeting factors with nascent polypeptide chains and ribosomes. Nat. Protoc. *8*, 2212-2239.

Berthold, N., Czihal, P., Fritsche, S., Sauer, U., Schiffer, G., Knappe, D., Alber, G., and Hoffmann, R. (2013). Novel apidaecin 1b analogs with superior serum stabilities for treatment of infections by Gram-negative pathogens. Antimicrob. Agents Chemother. *57*, 402-409.

Bray, N.L., Pimentel, H., Melsted, P., and Pachter, L. (2016). Near-optimal probabilistic RNA-seq quantification. Nat. Biotechnol. *34*, 525-527.

Bremer, H., and Dennis, P. (1996). Modulation of chemical composition and other parameters of the cell by growth rate. In *Escherichia coli* and *Salmonella*: Cellular and Molecular Biology,, F.C. Neidhardt, C.R. III, J.L. Ingraham, E.C.C. Lin, K.B. Low, B. Magasanik, W.S. Reznikoff, M. Riley, M. Schaechter, and H.E. Umbarger, eds. (Washington, D.C.: ASM Press), pp. 1553-1569.

Buskirk, A.R., and Green, R. (2017). Ribosome pausing, arrest and rescue in bacteria and eukaryotes. Philos. Trans. R. Soc. Lond. B, Biol. Sci. *372*, 1716.

Cabanas, M.J., Vazquez, D., and Modolell, J. (1978). Inhibition of ribosomal translocation by aminoglycoside antibiotics. Biochem. Biophys. Res. Commun. *83*, 991-997.

Casteels, P., Ampe, C., Jacobs, F., Vaeck, M., and Tempst, P. (1989). Apidaecins: antibacterial peptides from honeybees. EMBO J. *8*, 2387-2391.

Castle, M., Nazarian, A., Yi, S.S., and Tempst, P. (1999). Lethal effects of apidaecin on *Escherichia coli* involve sequential molecular interactions with diverse targets. J. Biol. Chem. *274*, 32555-32564.

Chambers, M.C., Maclean, B., Burke, R., Amodei, D., Ruderman, D.L., Neumann, S., Gatto, L., Fischer, B., Pratt, B., Egertson, J.*, et al.* (2012). A cross-platform toolkit for mass spectrometry and proteomics. Nat. Biotechnol. *30*, 918-920.

Dunn, J.G., Foo, C.K., Belletier, N.G., Gavis, E.R., and Weissman, J.S. (2013). Ribosome profiling reveals pervasive and regulated stop codon readthrough in *Drosophila melanogaster*. eLife *2*, e01179.

Florin, T., Maracci, C., Graf, M., Karki, P., Klepacki, D., Berninghausen, O., Beckmann, R., Vazquez-Laslop, N., Wilson, D.N., Rodnina, M.V.*, et al.* (2017). An antimicrobial peptide that inhibits translation by trapping release factors on the ribosome. Nat. Structur. Molec. Biol. *24*, 752-757.

Gagnon, M.G., Roy, R.N., Lomakin, I.B., Florin, T., Mankin, A.S., and Steitz, T.A. (2016). Structures of proline-rich peptides bound to the ribosome reveal a common mechanism of protein synthesis inhibition. Nucleic Acids Res. *44*, 2439-2450.

Gagnon, M.G., Seetharaman, S.V., Bulkley, D., and Steitz, T.A. (2012). Structural basis for the rescue of stalled ribosomes: structure of YaeJ bound to the ribosome. Science *335*, 1370-1372.

Gao, Y., Dasgupta, C., Huang, L., Song, R., Zhang, Z., and Zhang, L. (2019). Multi-omics integration reveals short and long-term effects of gestational hypoxia on the heart Development. Cells *8*.

Gao, Y., Yates, J.R. 3rd (2019). Protein analysis by shotgun proteomics. In Mass Spectrometry-Based Chemical Proteomics, W.A. Tao, Zhang, Y., ed. (Hoboken, USA: John Wiley & Sons), pp. 1-38.

Garza-Sanchez, F., Schaub, R.E., Janssen, B.D., and Hayes, C.S. (2011). tmRNA regulates synthesis of the ArfA ribosome rescue factor. Mol. Microbiol. *80*, 1204-1219.

Gessulat, S., Schmidt, T., Zolg, D.P., Samaras, P., Schnatbaum, K., Zerweck, J., Knaute, T., Rechenberger, J., Delanghe, B., Huhmer, A.*, et al.* (2019). Prosit: proteome-wide prediction of peptide tandem mass spectra by deep learning. Nat. Methods *16*, 509-518.

Graf, M., and Wilson, D.N. (2019). Intracellular antimicrobial peptides targeting the protein synthesis machinery. Adv. Exp. Med. Biol. *1117*, 73-89.

Huang, L., Aghajan, M., Quesenberry, T., Low, A., Murray, S.F., Monia, B.P., and Guo, S. (2019). Targeting translation termination machinery with antisense oligonucleotides for diseases caused by nonsense mutations. Nucleic Acid The.r *29*, 175-186.

Hwang, J.Y., and Buskirk, A.R. (2017). A ribosome profiling study of mRNA cleavage by the endonuclease RelE. Nucleic Acids Res. *45*, 327-336.

Ingolia, N.T., Ghaemmaghami, S., Newman, J.R., and Weissman, J.S. (2009). Genome-wide analysis in vivo of translation with nucleotide resolution using ribosome profiling. Science *324*, 218-223.

Ivanova, N., Pavlov, M.Y., Felden, B., and Ehrenberg, M. (2004). Ribosome rescue by tmRNA requires truncated mRNAs. J. Mol. Biol. *338*, 33-41.

Janssen, B.D., Garza-Sanchez, F., and Hayes, C.S. (2013). A-site mRNA cleavage is not required for tmRNA-mediated ssrA-peptide tagging. PLoS ONE *8*, e81319.

Juszkiewicz, S., Chandrasekaran, V., Lin, Z., Kraatz, S., Ramakrishnan, V., and Hegde, R.S. (2018). ZNF598 Is a Quality Control Sensor of Collided Ribosomes. Mol. Cell *72*, 469-481 e467.

Kasari, V., Pochopien, A.A., Margus, T., Murina, V., Turnbull, K., Zhou, Y., Nissan, T., Graf, M., Novacek, J., Atkinson, G.C.*, et al.* (2019). A role for the Saccharomyces cerevisiae ABCF protein New1 in translation termination/recycling. Nucleic acids research *47*, 8807-8820.

Kearse, M.G., Goldman, D.H., Choi, J., Nwaezeapu, C., Liang, D., Green, K.M., Goldstrohm, A.C., Todd, P.K., Green, R., and Wilusz, J.E. (2019). Ribosome queuing enables non-AUG translation to be resistant to multiple protein synthesis inhibitors. Genes Devel. *33*, 871-885.

Keeling, K.M., Xue, X., Gunn, G., and Bedwell, D.M. (2014). Therapeutics based on stop codon readthrough. Annu. Rev. Genomics Hum. Genet. *15*, 371-394.

Kolano, L., Knappe, D., Volke, D., Strater, N., and Hoffmann, R. (2020). Ribosomal target-binding sites of antimicrobial peptides Api137 and Onc112 are conserved among pathogensproviding new lead structures to develop novel broad-spectrum antibiotics. Chembiochem. doi: 10.1002/cbic.202000109.

Kong, A.T., Leprevost, F.V., Avtonomov, D.M., Mellacheruvu, D., and Nesvizhskii, A.I. (2017). MSFragger: ultrafast and comprehensive peptide identification in mass spectrometry-based proteomics. Nat. Methods *14*, 513-520.

Krizsan, A., Prahl, C., Goldbach, T., Knappe, D., and Hoffmann, R. (2015). Short proline-rich antimicrobial peptides inhibit either the bacterial 70S ribosome or the assembly of its large 50S subunit. Chembiochem *16*, 2304-2308.

Krizsan, A., Volke, D., Weinert, S., Strater, N., Knappe, D., and Hoffmann, R. (2014). Insect-derived proline-rich antimicrobial peptides kill bacteria by inhibiting bacterial protein translation at the 70S ribosome. Angew. Chem. Int. Ed. Engl. *53*, 12236-12239.

Li, G.W., Burkhardt, D., Gross, C., and Weissman, J.S. (2014). Quantifying absolute protein synthesis rates reveals principles underlying allocation of cellular resources. Cell *157*, 624-635.

Li, X., Yokota, T., Ito, K., Nakamura, Y., and Aiba, H. (2007). Reduced action of polypeptide release factors induces mRNA cleavage and tmRNA tagging at stop codons in Escherichia coli. Mol. Microbiol. *63*, 116-126.

Lin, J., Zhou, D., Steitz, T.A., Polikanov, Y.S., and Gagnon, M.G. (2018). Ribosome-Targeting Antibiotics: Modes of Action, Mechanisms of Resistance, and Implications for Drug Design. Annu. Rev. Biochem. *87*, 451-478.

Ling, J., Cho, C., Guo, L.T., Aerni, H.R., Rinehart, J., and Soll, D. (2012). Protein aggregation caused by aminoglycoside action is prevented by a hydrogen peroxide scavenger. Mol. Cell *48*, 713-722.

Ma, N.J., Hemez, C.F., Barber, K.W., Rinehart, J., and Isaacs, F.J. (2018). Organisms with alternative genetic codes resolve unassigned codons via mistranslation and ribosomal rescue. eLife *7*, e34878.

Mardirossian, M., Grzela, R., Giglione, C., Meinnel, T., Gennaro, R., Mergaert, P., and Scocchi, M. (2014). The host antimicrobial peptide Bac71-35 binds to bacterial ribosomal proteins and inhibits protein synthesis. Chem. Biol. *21*, 1639-1647.

Martin, M. (2011). Cutadapt removes adapter sequences from high-throughput sequencing reads. EMB Net J. *17*, 10-12.

Matsuo, Y., Tesina, P., Nakajima, S., Mizuno, M., Endo, A., Buschauer, R., Cheng, J., Shounai, O., Ikeuchi, K., Saeki, Y.*, et al.* (2020). RQT complex dissociates ribosomes collided on endogenous RQC substrate SDD1. Nat. Struct. Molec. Biol. *27*, 323-332

McGlincy, N.J., and Ingolia, N.T. (2017). Transcriptome-wide measurement of translation by ribosome profiling. Methods *126*, 112-129.

Meydan, S., Klepacki, D., Mankin, A.S., and Vázquez-Laslop, N. (2020). Identification of translation start sites in bacterial genomes. In Ribosome Profiling Methods in Molecular Biology, V.M. Labunskyy, ed. (New York Springer).

Meydan, S., Marks, J., Klepacki, D., Sharma, V., Baranov, P.V., Firth, A.E., Margus, T., Kefi, A., Vazquez-Laslop, N., and Mankin, A.S. (2019). Retapamulin-assisted ribosome profiling reveals the alternative bacterial proteome. Molecular cell *74*, 481-493.

Mohammad, F., Green, R., and Buskirk, A.R. (2019). A systematically-revised ribosome profiling method for bacteria reveals pauses at single-codon resolution. eLife *8*, 42591.

Moore, S.D., and Sauer, R.T. (2005). Ribosome rescue: tmRNA tagging activity and capacity in Escherichia coli. Mol. Microbiol. *58*, 456-466.

Mottagui-Tabar, S., Bjornsson, A., and Isaksson, L.A. (1994). The second to last amino acid in the nascent peptide as a codon context determinant. EMBO J. *13*, 249-257.

Oh, E., Becker, A.H., Sandikci, A., Huber, D., Chaba, R., Gloge, F., Nichols, R.J., Typas, A., Gross, C.A., Kramer, G.*, et al.* (2011). Selective ribosome profiling reveals the cotranslational chaperone action of trigger factor in vivo. Cell *147*, 1295-1308.

Olivier, N.B., Altman, R.B., Noeske, J., Basarab, G.S., Code, E., Ferguson, A.D., Gao, N., Huang, J., Juette, M.F., Livchak, S.*, et al.* (2014). Negamycin induces translational stalling and miscoding by binding to the small subunit head domain of the *Escherichia coli* ribosome. Proc. Natl. Acad. Sci. USA *111*, 16274-16279.

Parker, J. (1989). Errors and alternatives in reading the universal genetic code. Microbiol. Rev. *53*, 273-298.

Pimentel, H., Bray, N.L., Puente, S., Melsted, P., and Pachter, L. (2017). Differential analysis of RNA-seq incorporating quantification uncertainty. Nat. Methods *14*, 687-690.

Polikanov, Y.S., Aleksashin, N.A., Beckert, B., and Wilson, D.N. (2018). The mechanisms of action of ribosome-targeting peptide antibiotics. Front. Mol. Biosci. *5*, 48.

Polikanov, Y.S., Szal, T., Jiang, F., Gupta, P., Matsuda, R., Shiozuka, M., Steitz, T.A., Vazquez-Laslop, N., and Mankin, A.S. (2014). Negamycin interferes with decoding and translocation by simultaneous interaction with rRNA and tRNA. Mol. Cell *56*, 541-550.

Roy, R.N., Lomakin, I.B., Gagnon, M.G., and Steitz, T.A. (2015). The mechanism of inhibition of protein synthesis by the proline-rich peptide oncocin. Nat. Struct. Molec. Biol. *22*, 466-469.

Schmidt, A., Kochanowski, K., Vedelaar, S., Ahrne, E., Volkmer, B., Callipo, L., Knoops, K., Bauer, M., Aebersold, R., and Heinemann, M. (2016). The quantitative and condition-dependent Escherichia coli proteome. Nat. Biotechnol. *34*, 104-110.

Scocchi, M., Tossi, A., and Gennaro, R. (2011). Proline-rich antimicrobial peptides: converging to a non-lytic mechanism of action. Cell Mol. Life Sci. *68*, 2317-2330.

Seefeldt, A.C., Graf, M., Perebaskine, N., Nguyen, F., Arenz, S., Mardirossian, M., Scocchi, M., Wilson, D.N., and Innis, C.A. (2016). Structure of the mammalian antimicrobial peptide Bac7(1-16) bound within the exit tunnel of a bacterial ribosome. Nucleic Acids Res. *44*, 2429-2438.

Seefeldt, A.C., Nguyen, F., Antunes, S., Perebaskine, N., Graf, M., Arenz, S., Inampudi, K.K., Douat, C., Guichard, G., Wilson, D.N.*, et al.* (2015). The proline-rich antimicrobial peptide Onc112 inhibits translation by blocking and destabilizing the initiation complex. Nat. Struct. Molec. Biol. *22*, 470-475.

Subramaniam, A.R., Zid, B.M., and O'Shea, E.K. (2014). An integrated approach reveals regulatory controls on bacterial translation elongation. Cell *159*, 1200-1211.

Szklarczyk, D., Gable, A.L., Lyon, D., Junge, A., Wyder, S., Huerta-Cepas, J., Simonovic, M., Doncheva, N.T., Morris, J.H., Bork, P.*, et al.* (2019). STRING v11: protein-protein association networks with increased coverage, supporting functional discovery in genome-wide experimental datasets. Nucleic Acids Res. *47*, D607-D613.

Tate, W.P., Mansell, J.B., Mannering, S.A., Irvine, J.H., Major, L.L., and Wilson, D.N. (1999). UGA: a dual signal for 'stop' and for recoding in protein synthesis. Biochemistry (Biokhimiia) *64*, 1342-1353.

Thompson, J., Pratt, C.A., and Dahlberg, A.E. (2004). Effects of a number of classes of 50S inhibitors on stop codon readthrough during protein synthesis. Antimicrob. Agents Chemother. *48*, 4889-4891.

Tomoyasu, T., Mogk, A., Langen, H., Goloubinoff, P., and Bukau, B. (2001). Genetic dissection of the roles of chaperones and proteases in protein folding and degradation in the Escherichia coli cytosol. Mol. Microbiol. *40*, 397-413.

Traut, R.R., and Monro, R.E. (1964). The puromycin reaction and its relation to protein synthesis. J. Mol. Biol. *10*, 63-72.

Vazquez-Laslop, N., and Mankin, A.S. (2018). How macrolide antibiotics work. Trends Biochem. Sci. *43*, 668-684.

Vazquez-Laslop, N., Thum, C., and Mankin, A.S. (2008). Molecular mechanism of drug-dependent ribosome stalling. Mole. Cell *30*, 190-202.

Wang, L., Pulk, A., Wasserman, M.R., Feldman, M.B., Altman, R.B., Cate, J.H., and Blanchard, S.C. (2012). Allosteric control of the ribosome by small-molecule antibiotics. Nat. Struct. Molec. Biol. *19*, 957-963.

Wangen, J.R., and Green, R. (2020). Stop codon context influences genome-wide stimulation of termination codon readthrough by aminoglycosides. eLife *9*., 52611.

Weaver, J., Mohammad, F., Buskirk, A.R., and Storz, G. (2019). Identifying small proteins by ribosome profiling with stalled initiation complexes. mBio *10*, e02819-18.

Wilson, D.N. (2009). The A-Z of bacterial translation inhibitors. Crit. Rev. Biochem. Mol. Biol. *44*, 393-433.

Xu, T., Park, S.K., Venable, J.D., Wohlschlegel, J.A., Diedrich, J.K., Cociorva, D., Lu, B., Liao, L., Hewel, J., Han, X.*, et al.* (2015). ProLuCID: An improved SEQUEST-like algorithm with enhanced sensitivity and specificity. J. Proteomics *129*, 16-24.

Young, D.J., Guydosh, N.R., Zhang, F., Hinnebusch, A.G., and Green, R. (2015). Rli1/ABCE1 recycles terminating ribosomes and controls translationreinitiation in 3'UTRs in vivo. Cell 162, 872-884.

Zybailov, B., Coleman, M.K., Florens, L., and Washburn, M.P. (2005). Correlation of relative abundance ratios derived from peptide ion chromatograms and spectrum counting for quantitative proteomic analysis using stable isotope labeling. Anal. Chem. 77, 6218-6224.

Figure 1

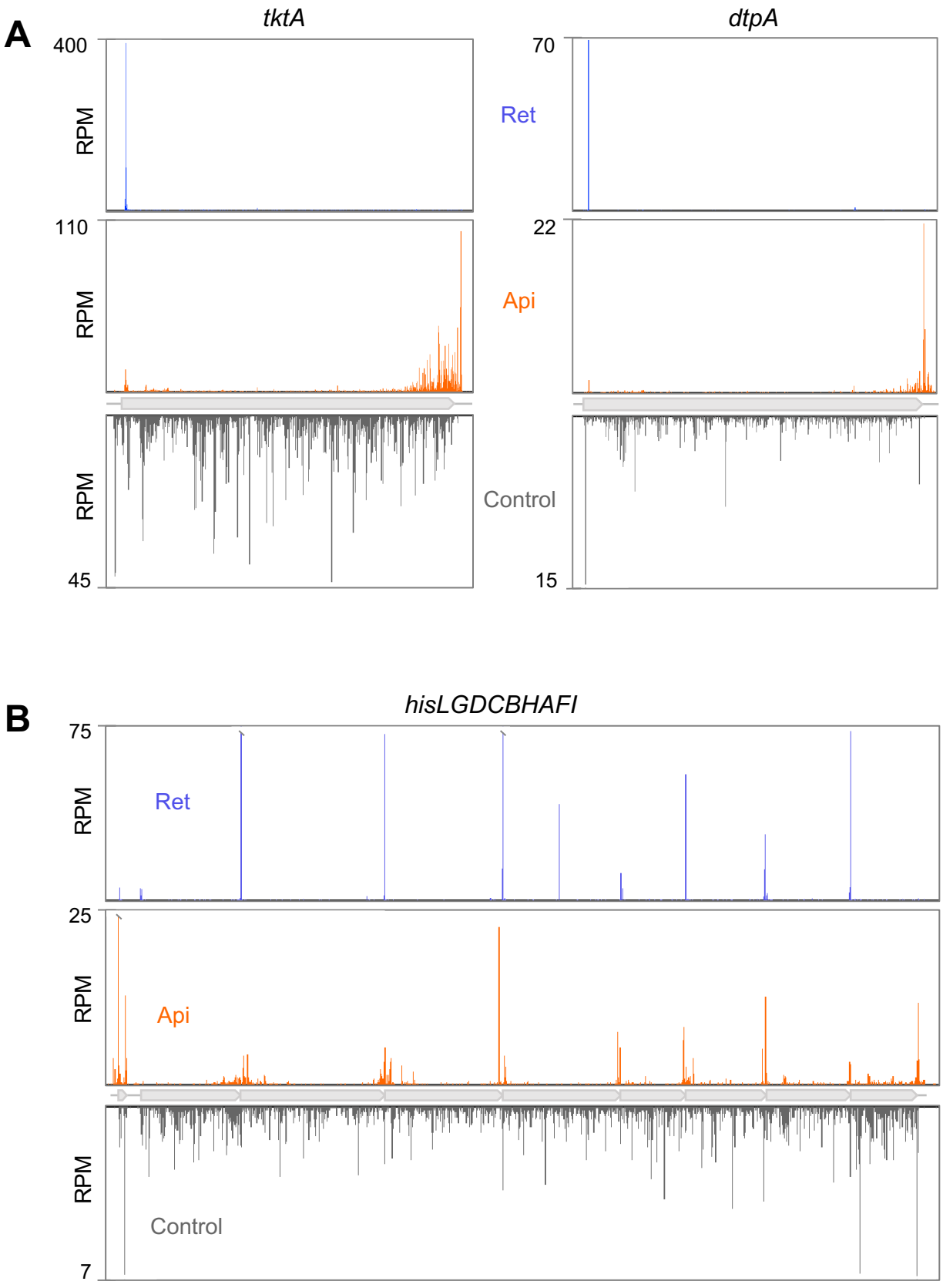
A
tktA
dtpA
400
RPM
70
Ret
110
RPM
22
Api
RPM
Control
45
15
B
hisLGDCBHAFI
75
RPM
Ret
25
RPM
Api
RPM
Control
7

Figure 2

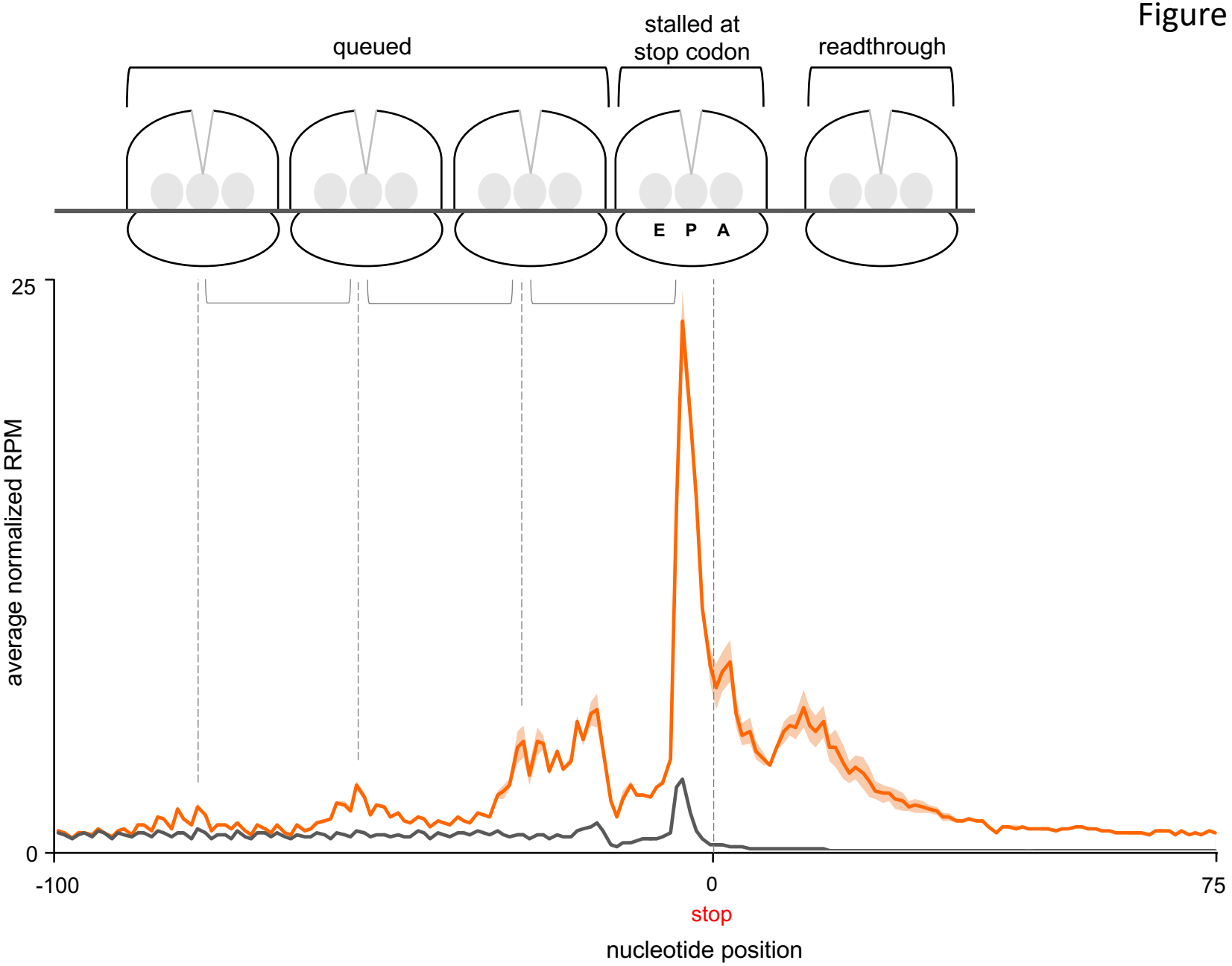
queued
stalled at
stop codon
readthrough
E P A
25
0
average normalized RPM
-100
0
75
stop
nucleotide position

Figure 3

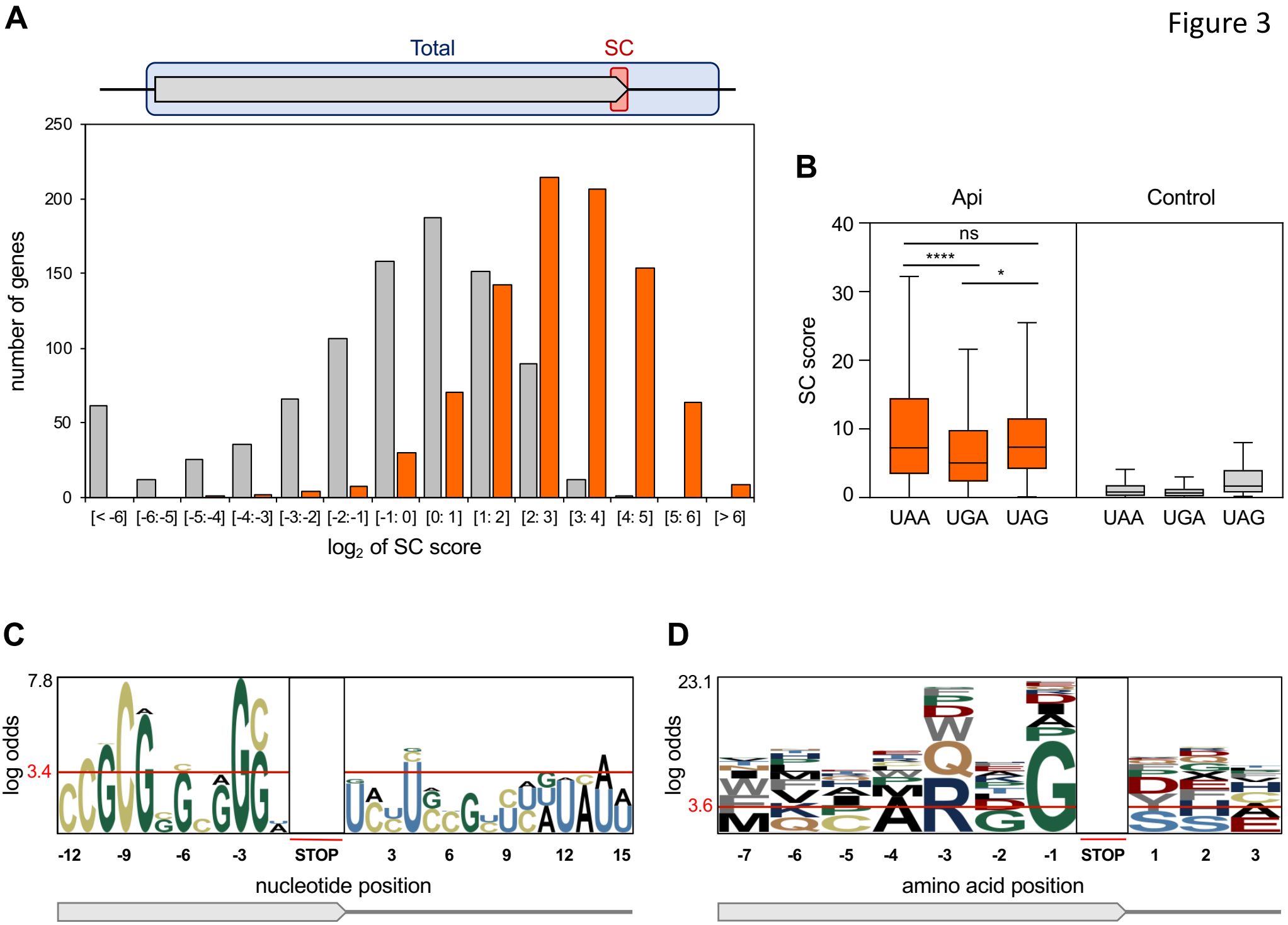
A
Total
SC
250
200
150
100
50
0
number of genes
[< -6] [-6:-5] [-5:-4] [-4:-3] [-3:-2] [-2:-1] [-1: 0] [0: 1] [1: 2] [2: 3] [3: 4] [4: 5] [5: 6] [> 6]
log2 of SC score
B
Api
Control
40
30
20
10
0
SC score
ns
****
*
UAA UGA UAG
UAA UGA UAG
C
7.8
3.4
log odds
-12 -9 -6 -3 STOP 3 6 9 12 15
nucleotide position
D
23.1
3.6
log odds
-7 -6 -5 -4 -3 -2 -1 STOP 1 2 3
amino acid position

Figure 4

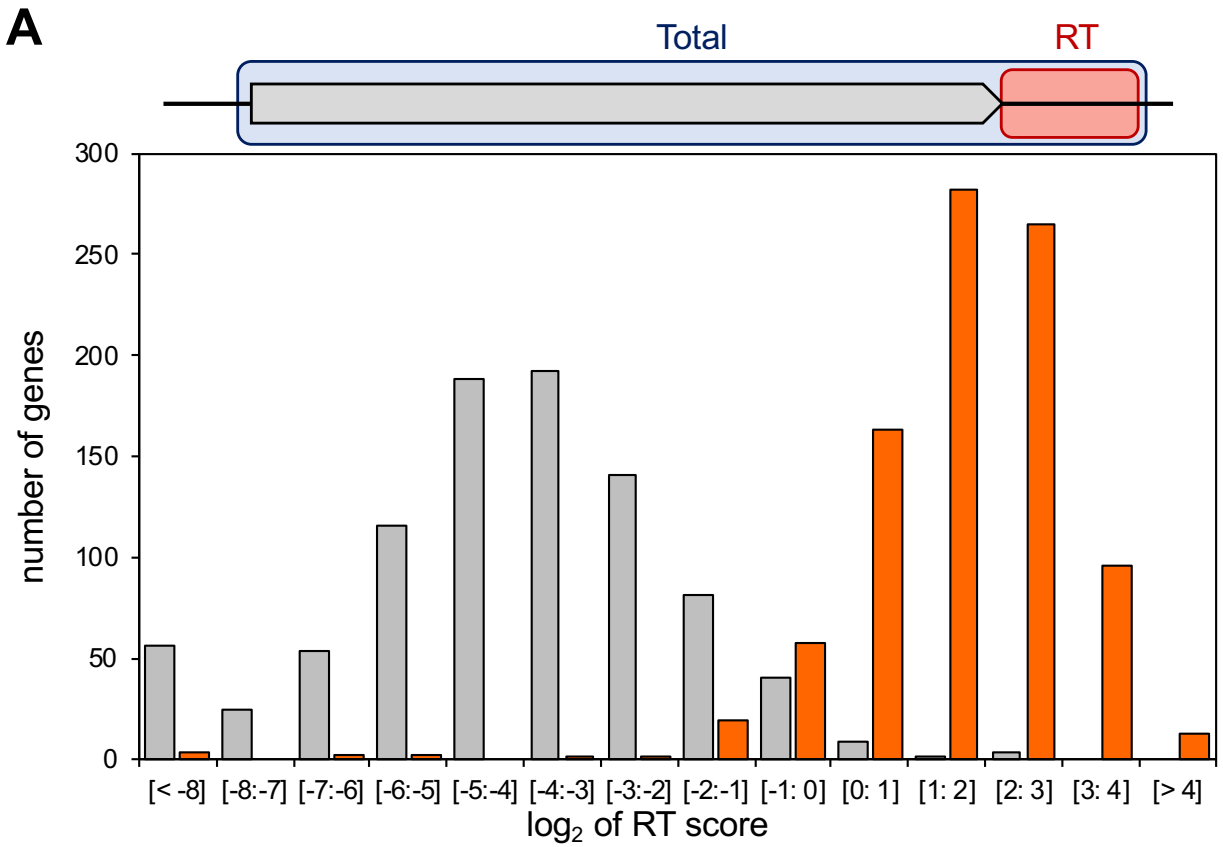
A
Total
RT
300
250
200
150
100
50
0
number of genes
[< -8]
[-8:-7]
[-7:-6]
[-6:-5]
[-5:-4]
[-4:-3]
[-3:-2]
[-2:-1]
[-1: 0]
[0: 1]
[1: 2]
[2: 3]
[3: 4]
[> 4]
log2 of RT score

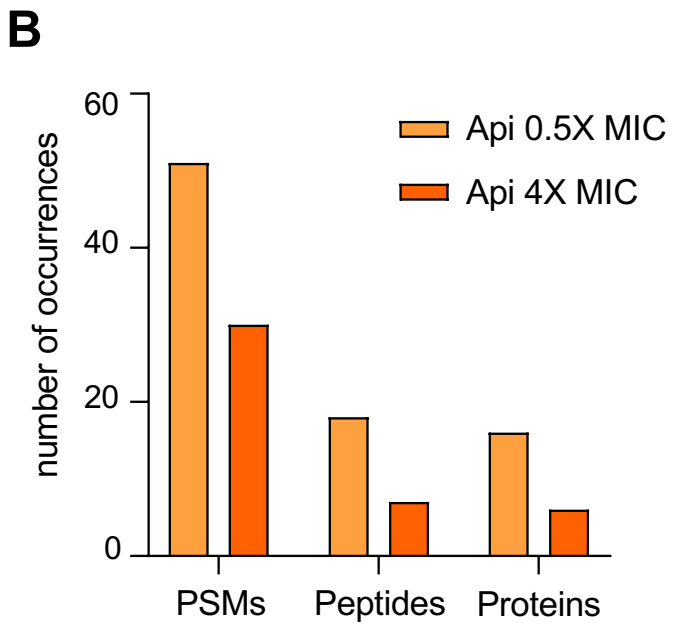
B
60
40
20
0
number of occurrences
Api 0.5X MIC
Api 4X MIC
PSMs
Peptides
Proteins

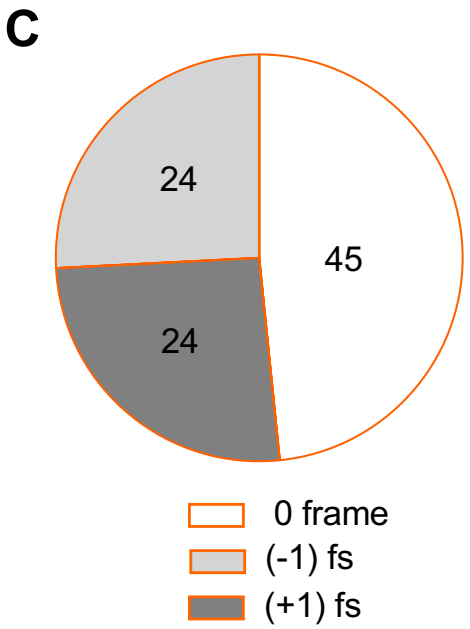
C
24
45
24
0 frame
(-1) fs
(+1) fs

Figure 5

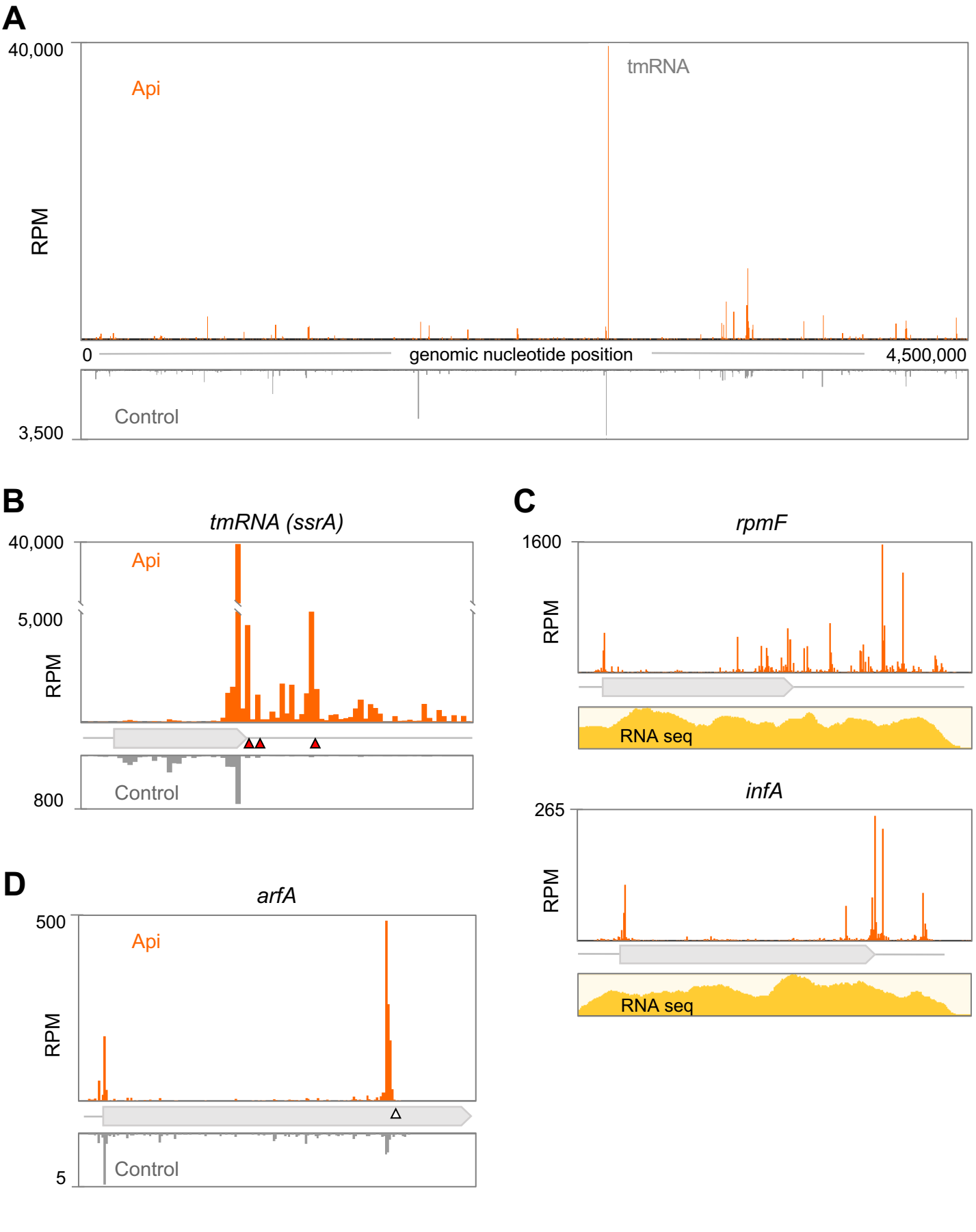
A
40,000
Api
tmRNA
RPM
0
genomic nucleotide position
4,500,000
Control
3,500
B
tmRNA (ssrA)
40,000
Api
5,000
RPM
Control
800
C
rpmF
1600
RPM
RNA seq
infA
265
RPM
RNA seq
D
arfA
500
Api
RPM
Control
5

SUPPLEMENTARY FIGURES AND TABLES

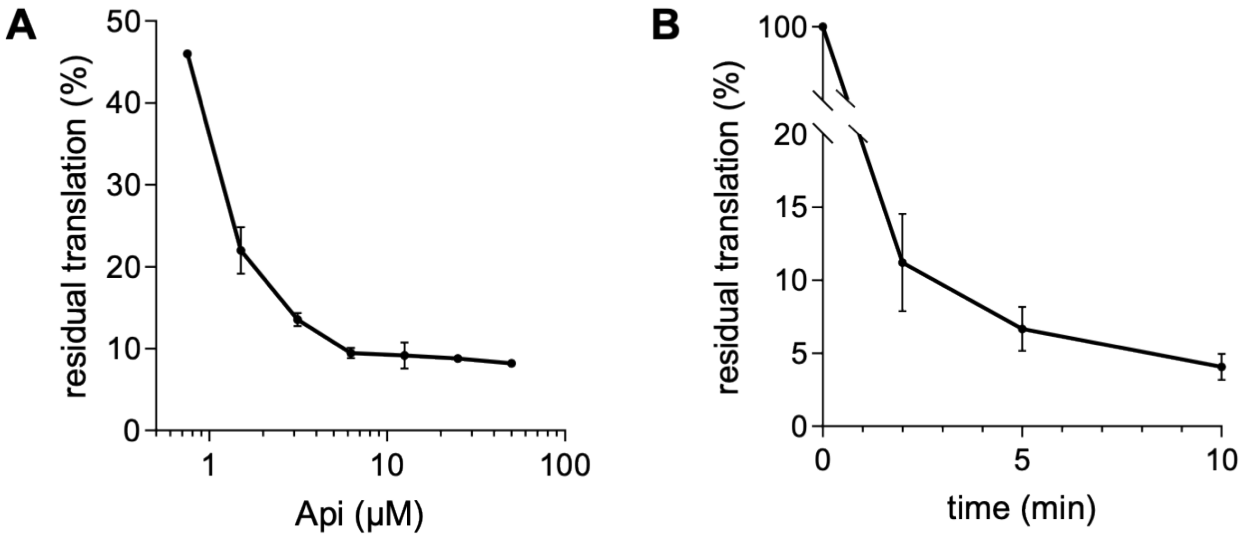

Associated to Figure 1

Figure supplement 1. Api inhibits global protein synthesis in *E. coli* cells. (**A**) Residual protein synthesis in BL21 Δ*tolC E. coli* cells exposed for 1 min to varying concentrations of Api137, as estimated by L-[^{35}S]-methionine incorporation into TCA-precipitable proteins. Incorporation of L-[^{35}S]-methionine in a sample devoid of Api was set as 100%. (**B**) Time course of inhibition of protein synthesis in cells exposed to 6.25 μM (4X MIC) of Api137. The shown data is the average of two independent experiments. Error bars indicate s.e.m.

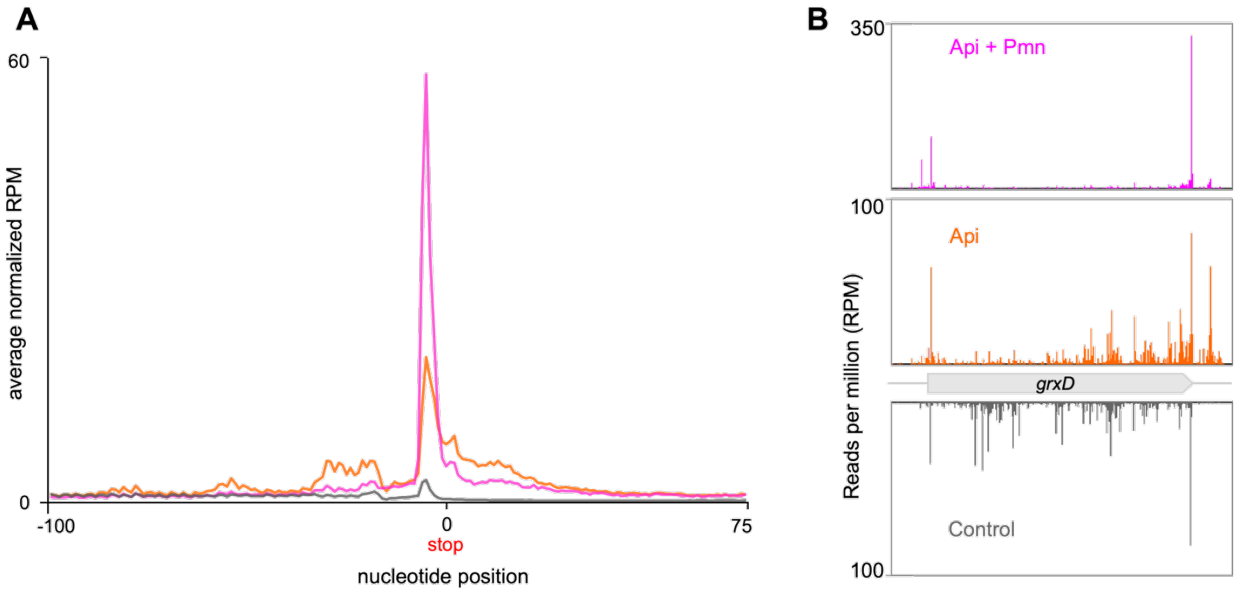

Associated to Figure 2

Figure supplement 1. Puromycin reduces the complexity of the Api-mediated ribosomal distribution patterns. (**A**) Metagene plots of the normalized ribosome density in the vicinity of the stop codons of genes in *E. coli* control cells (gray), cells exposed to Api (orange), or cells exposed to Api with subsequent puromycin (Pmn) treatment of the lysates (purple plot). (**B**) Ribosome density at the *grxD* ORF in the control cells or cells exposed to Api (without or with Pmn treatment).

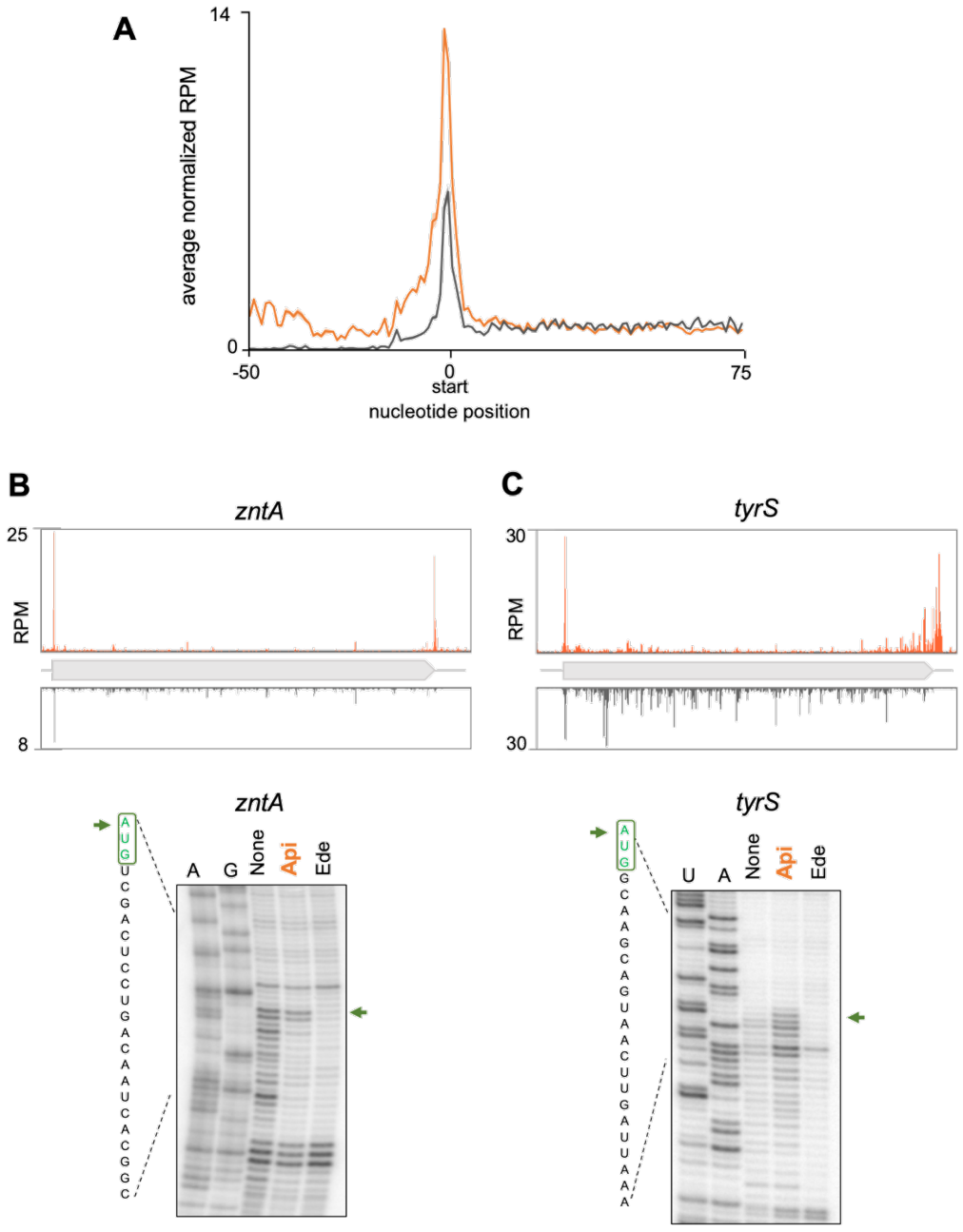

Associated to Figure 2

Figure supplement 2. Api moderately increases ribosome density at start codons. (**A**) Metagene plot of the normalized ribosome density in the vicinity of the start codons in *E. coli* cells treated (orange) or not (gray) with Api. (**B**) and (**C**) Examples of genes where Api causes ribosome stalling at the start codons during in vivo and in vitro translation. *Top*: Ribosome footprint density observed in Ribo-seq experiments. The start codons of the genes in Api-treated cells are indicated with green triangles. Bottom: toeprinting analysis showing ribosome stalling at the start codons (green arrows) during cell-free translation in the presence of 2mM of Api. The control antibiotic edein (Ede), which prevents ribosome binding to mRNA, was used to distinguish the toeprint bands originating from translating ribosomes.

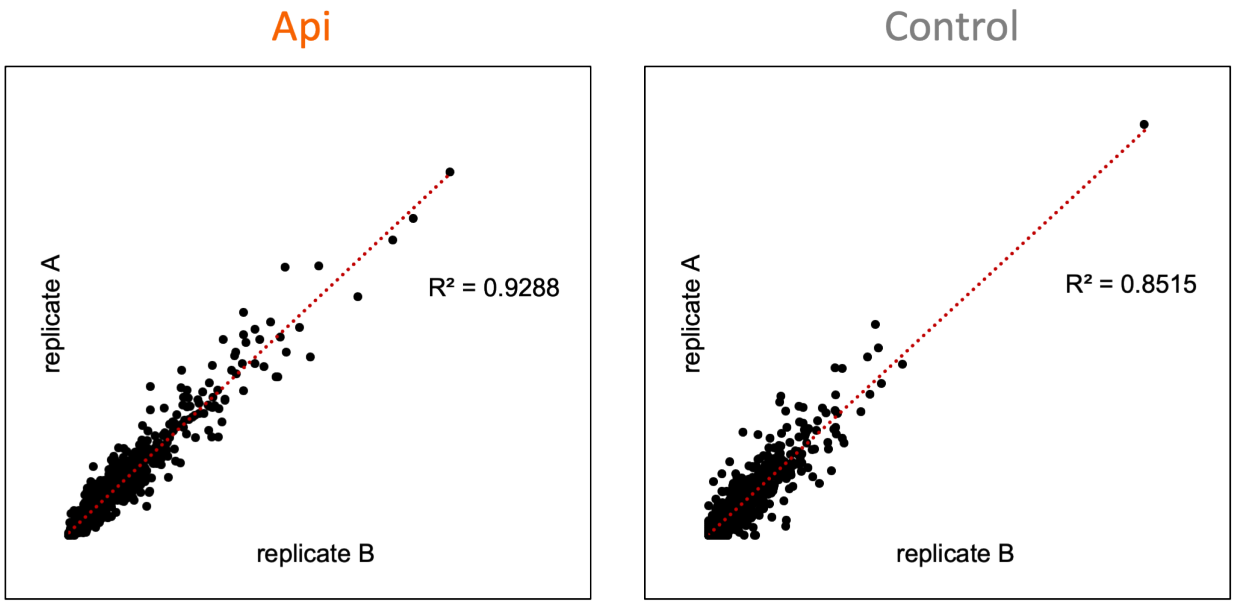

Associated to Figure 3

Figure supplement 1. Reproducibility of effects at stop codons. Correlation of the stop codon (SC) scores in Api-treated or control cells estimated from the Ribo-seq data obtained in two independent biological replicates.

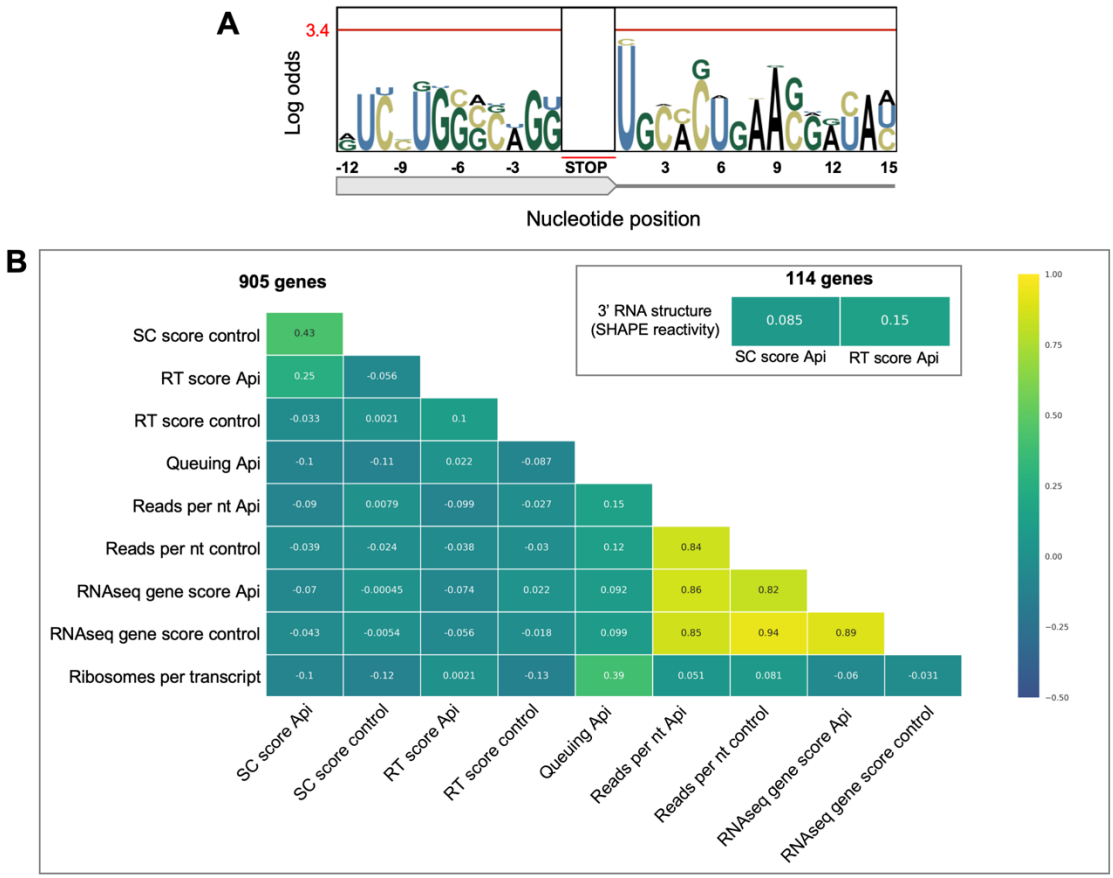

Associated to Figure 3

Figure supplement 2. Evaluation of cellular factors that could potentially contribute to Api-mediated ribosome arrest at stop codons. (**A**) pLogo analysis of nucleotide sequences in the vicinity of the termination sites of the 50% high-SC score vs. 50% low SC-score genes with UGA stop codon from Api treated cells. (**B**) Correlation between SC scores and readthrough (RT) scores (see Figure 4A in the main text) of genes from Api treated cells with various parameters calculated for the 905 well-separated (50 nt away from the nearest gene) and actively translated (ribosome footprint (rfp) density per nt ≥0.1) genes. Other than SC score and RT score, the following parameters were used: Asymmetry score: a parameter reflecting difference in the number of rfps in the first half of the gene relative to the number of rfps in the second half of the gene (Mohammad et al., 2019), used here as a metric for ribosome queuing; rfp density: the total number of rfps within an ORF (excluding the first and last 9 nts) divided by the length of an ORF; RNA-seq gene score: total number of reads per million mapped to an ORF; rfp per transcript: the number of rfp mapped to an ORF (excluding the first and last 9 nts) divided by the RNA-seq gene score (formally similar to translation efficiency metrics which is poorly applicable for the Api sample); 3' mRNA structure: the mean SHAPE reactivity of mRNA segment that includes 40 nt upstream and 10 nts downstream of the stop codon (Huang et al., 2019). The latter was calculated for 114 out of the aforementioned 905 genes, for which SHAPE-seq data were available.

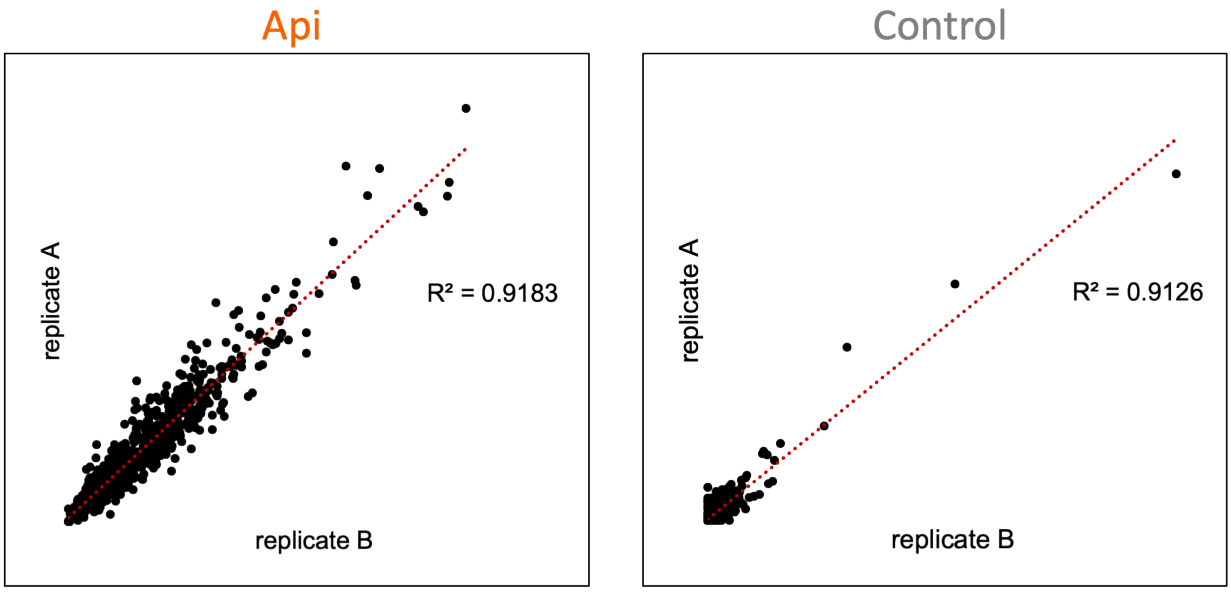

Associated to Figure 4

Figure supplement 1. Reproducibility of stop codon bypass effects. Correlation of the readthrough (RT) scores in Api-treated or control cells estimated from the Ribo-seq data obtained in two independent biological replicates.

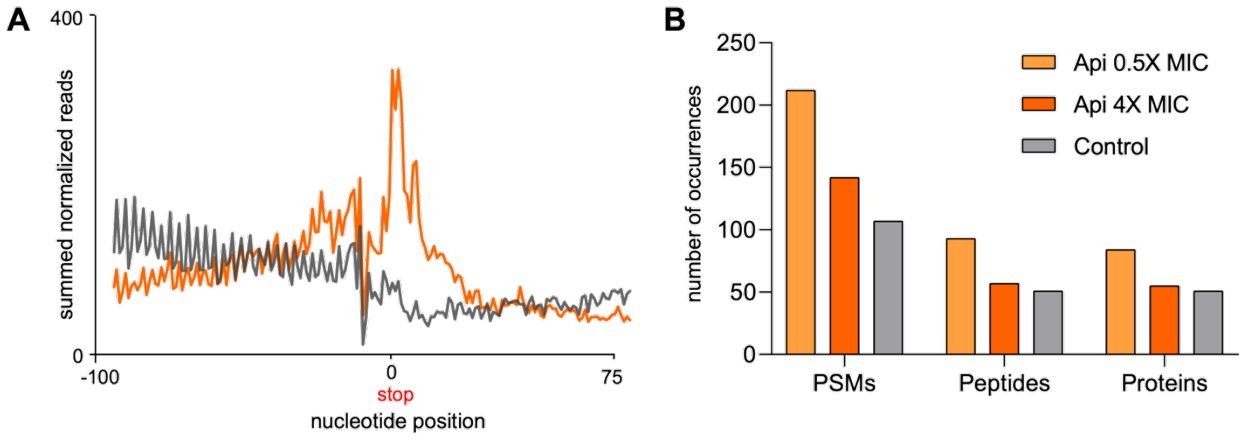

Associated to Figure 4

Figure supplement 2. In the Api-treated cells, ribosomes actively translate mRNA segments downstream from the stop codon of the main ORF. (**A**) Metagene plot of the ribosome footprints density in the vicinity of the first in-frame stop codon downstream from the main ORF termination codon in cells treated (orange) or not (gray) with Api. (**B**) Number of proteins with C-terminal extensions or PSMs and peptides counts belonging to the C-terminal extensions of proteins in the control and Api-treated cells identified by shotgun proteomics (a more relaxed criteria compared to those used for generation of the Figure 4B plots, see Materials and Methods).

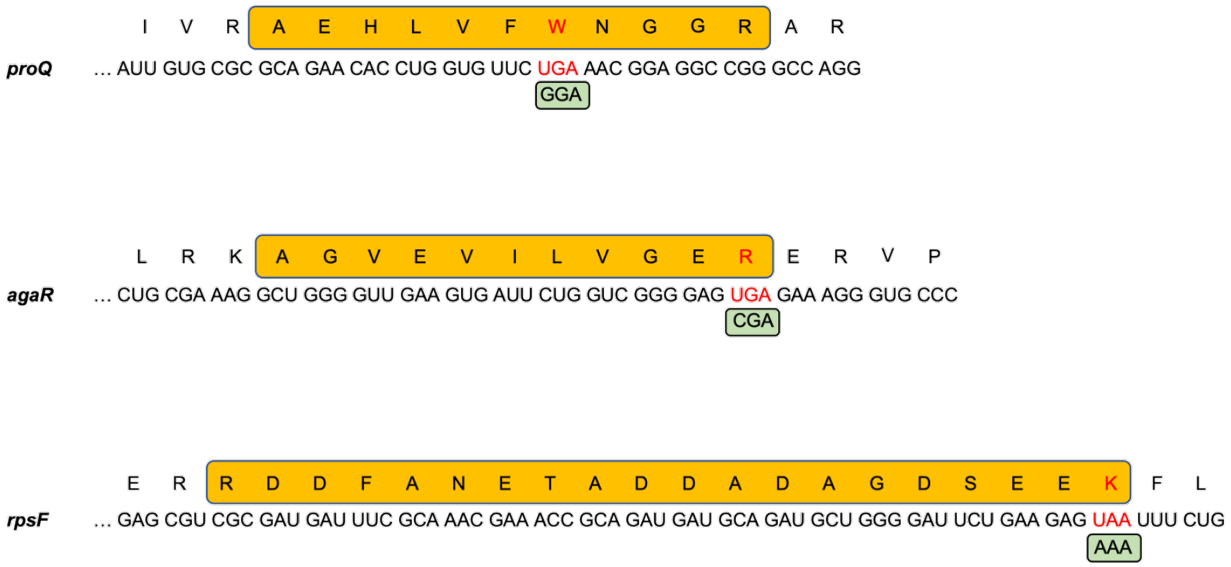

Associated to Figure 4

Figure supplement 3. Stop codon bypass by near-cognate aminoacyl-tRNA misincorporation. Api-induced 0-frame stop codon bypass occurs via decoding of the stop codon by a near-cognate aminoacyl-tRNA**.** Three peptides (yellow boxes), encoded by the mRNA sequences spanning the stop codons were identify by mass-spectrometry in the cells exposed to 0.5x MIC of Api. The nucleotide sequences of the 3'-proximal segments of the corresponding ORFs and amino acid sequences of the encoded proteins are shown. Stop codons and amino acids erroneously incorporated at stop codons are shown in red. The codon recognized by aminoacyl-tRNA that likely decoded the stop codon is shown in green boxes.

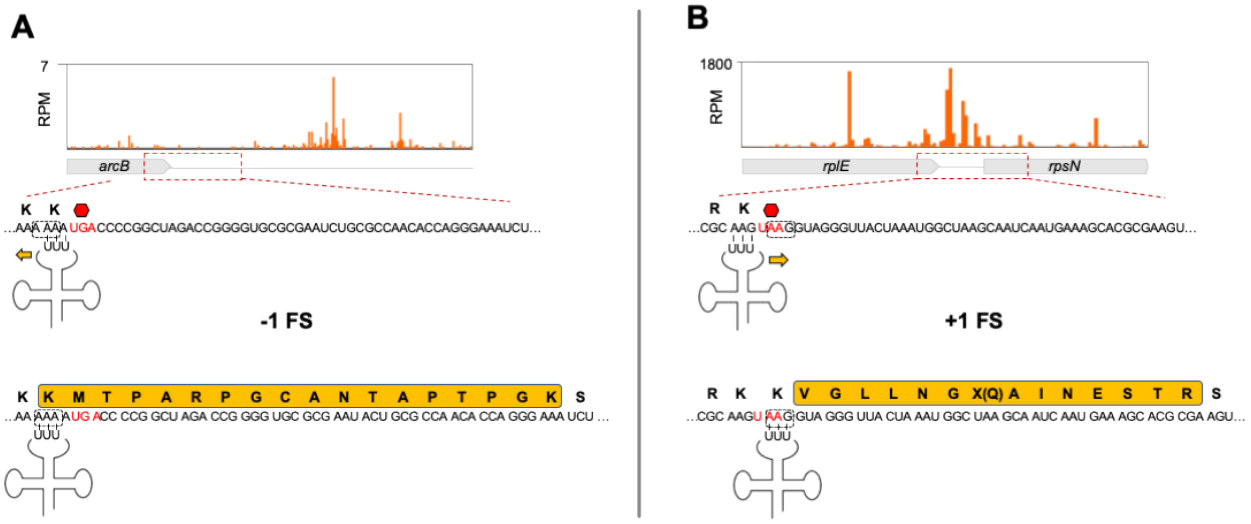

Associated to Figure 4

Figure supplement 4. Possible scenarios for stop codon bypass via frameshifting in Api-treated cells**. (A)** *Top*: Ribosome footprints density downstream of the *arcB* ORF in Api-treated cells. *Bottom*: Inability of the ribosome to rapidly terminate translation at the *arcB* UGA stop codon (red), due to Api-induced RF2 depletion, may allow for to a backwards shift of the peptidyl-tRNA^{Lys} occupying the last *arcB* sense codon AAA (boxed) within the slippery sequence, landing in an identical (-1) frame codon (boxed). (**B**) *Top*: Ribosome footprints density in the region downstream of the *rplE* ORF in Api-treated cells. *Bottom*: Slow termination of translation at the *rplE* UAA stop codon (red), may lead to repairing of the peptidyl-tRNA^{Lys} occupying the last *rplE* sense codon AAG to the nearby identical codon in a (+1) frame (boxed). In (A) and (B), the amino acid sequences of the tryptic peptide identified by shotgun proteomics in cells treated with Api are highlighted in yellow. Note that the stop codon within the (+1) frame downstream of *rplE* is apparently bypassed by misincorporation of a near-cognate Gln-tRNA$^{(UUG)}$. Also of note, the same tryptic peptide as the one encoded in the mRNA segment downstream of the *arcB* gene could be also identified in untreated cells.

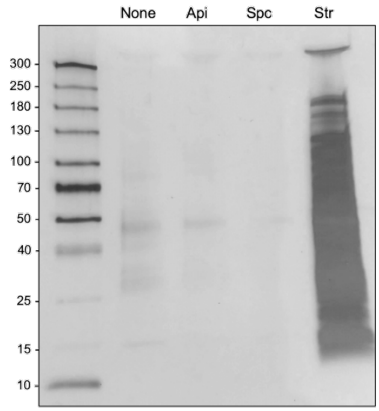

Associated to Figure 4

Figure supplement 5. Api treatment does not lead to pronounced protein aggregation in *E. coli* cells. Cells were treated or not with apidaecin (Api), spectinomycin (Spc), or streptomycin (Str) at 2-fold the respective MICs for 30 minutes. Protein aggregates were isolated, separated by SDS-PAGE and visualized by silver staining. Spc and Str are verified positive and negative controls in these conditions (Ling et al., 2012).

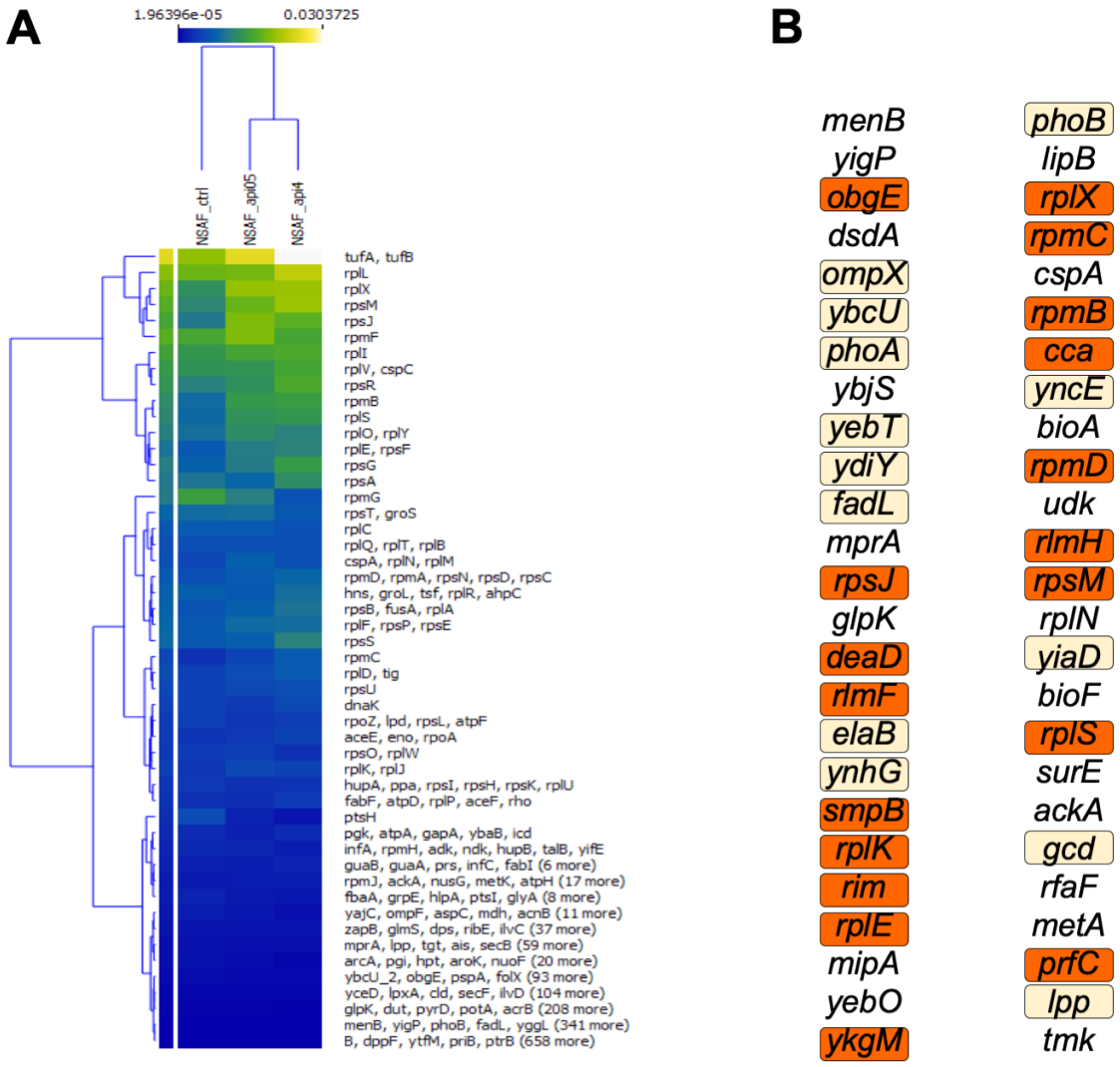

Associated to Figure 5

Figure supplement 1. (A) Api-induced changes in protein abundance. Changes in relative protein abundance in *E. coli* cells exposed to 0.5x MIC and 4x MIC of Api relative to the untreated control cells. The heatmap scale reflects length-adjusted fractional abundance of the protein in the total protein sample (blue – less abundant, yellow – more abundant). Genes are clustered using hierarchical k-mean clustering algorithm. The color represents the relative abundance of each protein or protein cluster using normalized spectral abundance factor (NSAF). **(B)** Top 50 proteins showing significant increase in abundance in the cells treated with 0.5x MIC of Api relative to the untreated control. Proteins related to translation are highlighted in orange. Periplasmic, inner- and outer-membrane proteins are highlighted in beige.

Minimal inhibitory concentration

***E. coli* strain**	**Api MIC (μM)**
BW25113 (wt)	12.5
BW25113 Δ*arfA*	6.25
BW25113 Δ*arfB*	12.5
BW25113 Δ*smpB*	25

Associated to Figure 5

Figure supplement 2. MIC concentrations of Api against *E. coli* BW25113 cells lacking individual ribosome rescue systems. SmpB protein is essential for the operation of the tmRNA-based ribosome rescue system (Buskirk and Green, 2017). All the tested strains were acquired from the Keio collection (Baba et al., 2006) and verified by PCR.

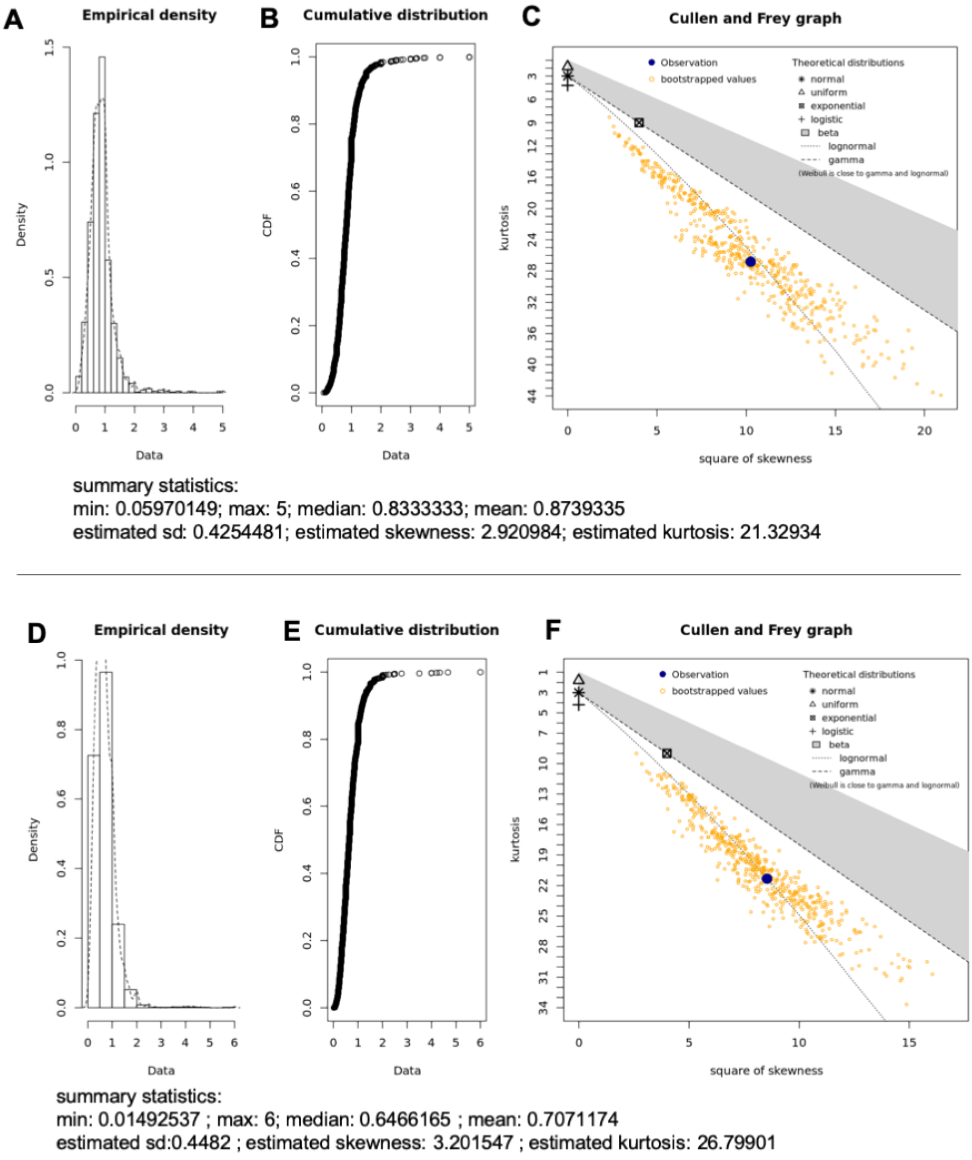

Associated to Figure 5

Figure supplement 3. Modelling the distribution of NSAF ratios between (**A-C**) Api 0.5x MIC and control or (**D-F**) Api 4x MIC and control samples. (**A,D**), Empirical density graphs; (**B,E**) cumulative distribution graphs; (**C,F**) Cullen and Frey graphs of the NSAF ratios between Api samples and control. The analysis shows that sample ratios fit best gamma distribution.

Supplementary Information references

Baba, T., Ara, T., Hasegawa, M., Takai, Y., Okumura, Y., Baba, M., Datsenko, K.A., Tomita, M., Wanner, B.L., and Mori, H. (2006). Construction of *Escherichia coli* K-12 in-frame, single-gene knockout mutants: the Keio collection. Mol. Syst. Biol. *2*, 2006 0008.

Buskirk, A.R., and Green, R. (2017). Ribosome pausing, arrest and rescue in bacteria and eukaryotes. Philos. Trans. R. Soc. Lond. B Biol. Sci *372*, 1716

Huang, L., Aghajan, M., Quesenberry, T., Low, A., Murray, S.F., Monia, B.P., and Guo, S. (2019). Targeting translation termination machinery with antisense oligonucleotides for diseases caused by nonsense mutations. Nucleic Acid Ther, *29*, 175-186.

Ling, J., Cho, C., Guo, L.T., Aerni, H.R., Rinehart, J., and Soll, D. (2012). Protein aggregation caused by aminoglycoside action is prevented by a hydrogen peroxide scavenger. Mol. Cell *48*, 713-722.

Mohammad, F., Green, R., and Buskirk, A.R. (2019). A systematically-revised ribosome profiling method for bacteria reveals pauses at single-codon resolution. eLife *8*, e42591